

**ON A 3GPP RAY-BASED SPATIAL CHANNEL MODEL FOR MIMO SYSTEM
EMULATION: IMPLEMENTATION AND EVALUATION**

By

SABARISH KARTHIK VIVEK SARATHY

A thesis submitted to the

Graduate School - New Brunswick

Rutgers, The State University of New Jersey

in partial fulfillment of the requirements

for the degree of

Master of Science

Graduate Program in Electrical and Computer Engineering

Written under the direction of

Prof. Dr. Predrag Spasojevic

and approved by

New Brunswick, New Jersey

January, 2013

ABSTRACT OF THE THESIS

ON A 3GPP RAY-BASED SPATIAL CHANNEL MODEL FOR MIMO SYSTEM EMULATION: IMPLEMENTATION AND EVALUATION

by SABARISH KARTHIK VIVEK SARATHY

Thesis Director:

Prof. Dr. Predrag Spasojevic

The mitigation of random effects in a wireless communication channel is a problem considered for many years. In the present day context, given the ever increasing need for, and growth of, bandwidth intensive applications like streaming wireless HD video on fast moving user equipment (UEs, i.e., user communication devices), this issue has intensified from being a theoretical pursuit to a must-be-solved practical endeavor. In that regard, the ability to accurately model the outdoor (or indoor) propagation conditions in a laboratory setting becomes vital to validating state-of-the-art wireless standards and the devices that derive from them. Laboratory-based analysis is a significant catalyst in reducing the time-to-market for telecom equipment manufacturers. Modeling a wireless channel has been a topic under quite a bit of study. This has progressed from the Jakes model developed for single antenna systems to the correlation and ray-based models used for multiple antenna systems. The models prescribed by the 3rd Generation Partnership Project (3GPP) in its standards, like the ray-based model, aim to realistically reproduce channel environments in software and

hardware, by incorporating all the variables that characterize any particular fading scenario.

In this thesis, the technical report produced by 3GPP detailing the Spatial Channel Modeling (SCM) for multiple input multiple output (MIMO) simulations is followed closely as a basis for developing a real-time channel emulator on a National Instruments (NI) based Real Time (RT) Platform. First, a general purpose channel emulator is described in terms of its structure and functionality and currently known channel models are briefly investigated. Next, the spatial channel model in the standard is described in detail along with the reasons for choosing to use it in the thesis. All the parameters involved are defined, and the formula for constructing the channel is carefully investigated. Next, the channel emulator built on the National Instruments LabVIEW platform is described along with both the changes and modifications made to the design parameters so as to adapt it to the operating constraints of the RT platform. The spatial and temporal characteristics of the model are also described and plotted. Finally, the model is tested for reliability by methodically changing the various channel parameters and observing their effects on an Orthogonal Frequency Division Multiplexing (OFDM) test vector by generating BER performance plots in MATLAB. Diversity schemes are also employed to improve rate performance.

Acknowledgements

I would like to thank Prof. Dr. Predrag Spasojevic for serving as my thesis advisor and for mentoring me through the course of this thesis study. He has been patient enough to answer all of my queries, which has helped increase my understanding of the subject, and has expertly steered me through this important undertaking. I am grateful to him for helping me achieve a successful outcome to my research efforts.

I would also like to thank my friends and colleagues Abhishek Bindiganavile, Ajay Iyer and Swapnil Mhaske who have helped me at various stages with a variety of issues that I have faced. I am also grateful to Kareem Bonna and Mr. John Scafidi for helping me with access to laboratory facilities needed to conduct this study.

Table of Contents

Abstract	ii
Acknowledgements	iv
List of Tables	viii
List of Figures	ix
1. Introduction	1
1.1. Need for channel emulation	1
1.2. The state of the art	2
1.3. Scope of the thesis	5
2. The Ray Tracing Model	7
2.1. Background	7
2.1.1. Power Azimuth Spectrum (PAS) and Power Delay Spectrum (PDS)/Power Delay Profile (PDP)	8
2.1.2. Spatial Correlation in MIMO Arrays	10
2.1.3. PAS distributions	12
2.1.3.1. Uniform PAS model	12
2.1.3.2. Truncated Laplacian PAS model	14
2.1.4. Base Station Spatial Parameters	15
2.1.4.1. BS Antenna Pattern	15
2.1.4.2. Per-path BS AS	16
2.1.4.3. Per-path BS AoD	16
2.1.4.4. Per-path BS PAS	17
2.1.5. Mobile Station Spatial Parameters	17
2.1.5.1. MS Antenna Pattern	17

2.1.5.2. Per-path MS AS	17
2.1.5.3. Per-path MS AoA	18
2.1.5.4. Per-path MS PAS	18
2.1.5.5. MS Direction of Travel (DoT)	18
2.1.5.6. Per-path Doppler Spectrum	18
2.2. Scope of the Ray Tracing Model	19
2.3. The Spatial Snapshot of the Channel	21
2.4. Generation of channel coefficients	24
3. LabVIEW Implementation of the Channel Model	28
3.1. Overview	28
3.2. LabVIEW Virtual Instruments (VIs)	31
3.3. The National Instruments Real-Time System	33
4. Simulations and Performance Evaluation	35
4.1. Purpose of the simulations	35
4.2. Simulation Results	40
4.2.1 SISO	40
4.2.2 2 x 2 MIMO	42
5. Conclusions and Future Work	53
Appendix A	55
Appendix B	57
Appendix C	58
Appendix D	59
Appendix E	61

References	62
------------------	----

List of Tables

4.1.	A summary of the transmission parameters	38
4.2.	A summary of the channel parameters	39
4.3.	Parameters of the ITU PDPs	40

List of Figures

1.1.	A 2x2 MIMO system	2
1.2.	Top level design approach of a typical channel emulator	3
2.1.	A multipath cluster model	7
2.2.	Illustration of the multipaths in a multi-antenna setting	9
2.3.	Illustration of PAS and PDS	10
2.4.	Path difference between signals arriving at 2 antenna elements	11
2.5.	Illustration of a uniform PAS with $\phi_0=0$ degrees and $\Delta\phi=60$ degrees	14
2.6.	Spatial Correlation as a function of antenna spacing for a single cluster	14
2.7.	Antenna Pattern for 3-sector cells	16
2.8.	Illustration of the fundamental angular parameters of the SCM	21
3.1.	Overview of the LabVIEW system implementation blocks	28
3.2.	A partial snapshot of the control block user interface	29
3.3.	Real-time development tools	35
3.4.	Illustration of the system implementation inside the RT platform	37
4.1.	BER for the modified pedestrian A profile with LOS off	41
4.2.	BER for the vehicular A profile	41
4.3.	BER for the pedestrian B profile	42
4.4.	Illustration of the dependence of spatial correlation on mean AoA	43
4.5.	BER for the NLOS modified pedestrian profile for varying antenna spacing at the BS	44
4.6.	BER for a single tap channel for varying mean AoA	44
4.7.	BER for a spatial diversity scheme for an antenna spacing of 0.5λ in a 3 sector case	45
4.8.	BER for a spatial diversity scheme for an antenna spacing of 4λ in a 3 sector case	46

4.9. BER for a spatial diversity scheme for an antenna spacing of 10λ in a 3 sector case	46
4.10. BER for a beamforming MIMO system for 0.5λ antenna spacing	47
4.11. Spatial correlation at the BS as a function of varying antenna spacing for AS= 2 deg	48
4.12. Spatial correlation at the BS as a function of varying antenna spacing for AS= 5 deg	49
4.13. Spatial correlation at the BS as a function of varying AoD for AS=5 deg	50
4.14. Spatial correlation at the BS as a function of varying AoD for AS=2 deg	50
4.15. Spatial correlation at the BS as a function of varying AoD for 0.5λ inter antenna spacing	51
4.16. Temporal correlation at the MS for varying distance traveled	52

Chapter 1

Introduction

1.1 Need for channel emulation

Wireless communication techniques have, since their inception and materialization, been trying to overcome the overarching effects of the wireless medium, the channel. Clever and complicated counter measures have been in continuous deployment on both the transmitter and receiver sides to alleviate the multipath fading, signal distortion and interference caused by the channel. With advanced radio standards using capacity ameliorating technologies like MIMO and OFDM constantly being drafted to cater to the needs of the modern day user - one who poses a demand for high data rate content transfer in the form of interactive and streaming multimedia applications - the process of testing and validation of these standards in the light of the deterring channel effects is of utmost importance. Since nearly every aspect of wireless communication pretty much revolves around the channel, a system that can repeatedly replicate the actual conditions of a propagating medium in a controlled laboratory setting is necessary to achieve cross-layer validation of the techniques and algorithms in the standards. Such a system is the channel emulator.

The channel emulator does more than just 'simulate' a wireless channel. It reproduces the exact scattering, multipath and Doppler characteristics of any particular 'scenario' and the convolution of the signal as it passes through it, in real-time. This means that it is not an offline operation where the transmitted samples are stored and

then filtered with the channel at one go, akin to block convolution, but rather a sample-by-sample implementation in real-time.

Fig.1.1 shows a generic MIMO system. Each h_{ij} represents a channel coefficient between a pair of transmitter and receiver antennas. It is the fundamental quantity of interest in this thesis and is what is to be determined as a function of a plethora of parameters.

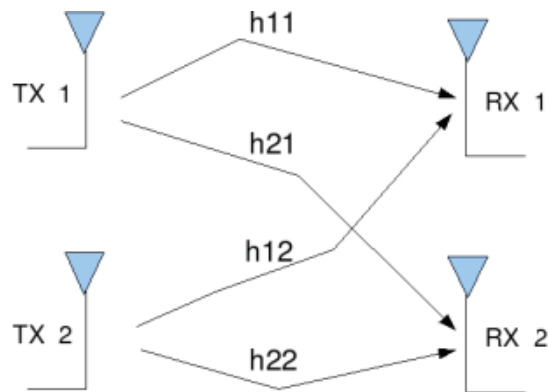


Figure 1.1: A 2 x 2 MIMO system.

1.2 The state of the art

Literature suggests that a full-fledged implementation of a channel emulator actually occurs in two steps. Because of the time critical nature of the convolution operation, it is done on high speed hardware, while the computation of the channel coefficients occurs using a non real time application on a host PC [1][2][3][4], as shown in fig.1.2. This division of activities enables efficiency as the hardware is not strained with excessive computations.

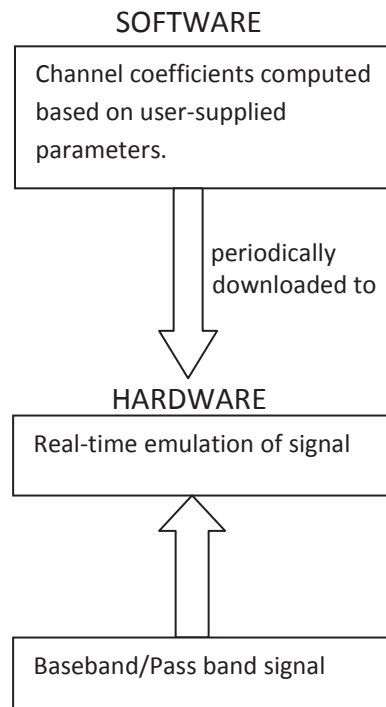


Figure 1.2 : Top level design approach of a typical channel emulator.

The convolution operation has been a topic of much study. While much of the research for single input single output (SISO) as well as multiple input multiple output (MIMO) systems has focused on FIR filter implementation[1][4], [2][3] suggest a frequency domain approach for the MIMO case. The authors mainly argue that while the time- domain method is well suited for SISO systems with short delay spreads, the complexity scales quadratically with the MIMO array size. Also, by comparing academically published emulators, they show that there exists a tradeoff between the average number of 'taps' per sub-channel and the number of sub-channels that can be supported in the FIR implementation, owing to the limited hardware resources. Their results show that an FFT based approach exhibits an initial fixed complexity which grows

at a slower rate as a function of the MIMO array size as compared to the FIR method, and that it is independent of the number of taps.

With regard to the generation of the channel coefficients for a MIMO system, three major approaches are followed as is detailed in [5] - the ray based approach, the scattering model and the correlation model. In the ray based approach, free space propagation, reflection, diffraction and scattering are modeled on a path by path basis, and then the planar wave fronts are summed. While it produces accurate results for both indoor and outdoor modeling, complexity becomes an issue for large scale system simulations. The scattering model assumes a particular distribution of scatterers and generates the channel based on the interaction of scatterers and planar wave fronts. Its main drawbacks are its complexity and large simulation time. Finally the correlation model, although simple to implement, decouples the spatial and temporal characteristics of the channel meaning their joint statistics are not preserved. But because of its relatively easy implementation, many hardware based emulators encountered in literature, including [1][3] showcase the correlation based method by using the Kronecker channel model [3][6]. Basically, this method operates by multiplying a matrix of independent and identically distributed (i.i.d) values with the Kronecker product of the spatial correlation matrices of the transmitter and receiver to generate the final channel matrix, as shown below[2]:

$$H = \{R_{tx} \otimes R_{rx}\}^{\frac{1}{2}} H_{i.i.d} \quad (1.1)$$

The above representation is for the non line-of-sight (NLOS) case. When a line of sight (LOS) exists, the composite matrix is as follows:

$$H_l = \sqrt{P_l} \left(\sqrt{\frac{K_l}{K_l + 1}} H_{l,LOS} + \sqrt{\frac{1}{K_l + 1}} H_{l,NLOS} \right) \quad (1.2)$$

where P_l is the power, K_l is the Rice K factor, $H_{l,LOS}$ and $H_{l,NLOS}$ are the LOS and NLOS channel matrices respectively, all for the l^{th} tap. In this case, the left-hand-side of (1.1) becomes $H_{l,NLOS} \cdot H_{l,LOS}$ is generated independently using the specified Doppler spectrum.

1.3 Scope of the thesis

This thesis focuses on the development of a channel emulator in LabVIEW for deployment to an RT system, based on the ray based technique. The reasons for choosing this method are:

- i) The existence of a detailed technical document [7] published by 3GPP outlining the procedures and guidelines for this method.
- ii) Simplicity of implementation for MIMO arrays of order up to 2 X 2 and since hardware implementation is not considered in this work.
- iii) The ability to model SISO and MIMO systems with no change to the structure of the model.
- iv) Maintenance of the joint statistics of the temporal and spatial domains.
- v) Intuitiveness of the model. The model paints a comprehensible picture of the actual propagating conditions and operates on the fundamental notion of the summing and canceling of wavefronts, taking into account power distributions and physical

angles. Therefore it is the author's belief that such a model is more intuitive compared to the not-so straightforward matrix operations of the correlation method.

The 3GPP technical document also specifies a number of options that can be included in the channel model, only one of which has been implemented - the LOS option. The goal of the thesis is to build a simple reliable emulator, incorporating all the defining characteristics of the channel, and that can be used to verify system level algorithms. Also, because it is done in LabVIEW, future migration to hardware is also possible thanks to the holistic hardware integration options provided by National Instruments.

The rest of the thesis is organized as follows: Chapter 2 describes the ray based model. Chapter 3 explains the implementation details in LabVIEW and Chapter 4 describes the simulation parameters and the performance graphs. Chapter 5 outlines the future work.

Chapter 2

The Ray Tracing Model

2.1 Background

Broadly, the ray tracing model works by the linear superposition of individual paths that travel from the base station (BS) to the mobile station (MS). Figure 2.1 illustrates a typical multipath scenario.

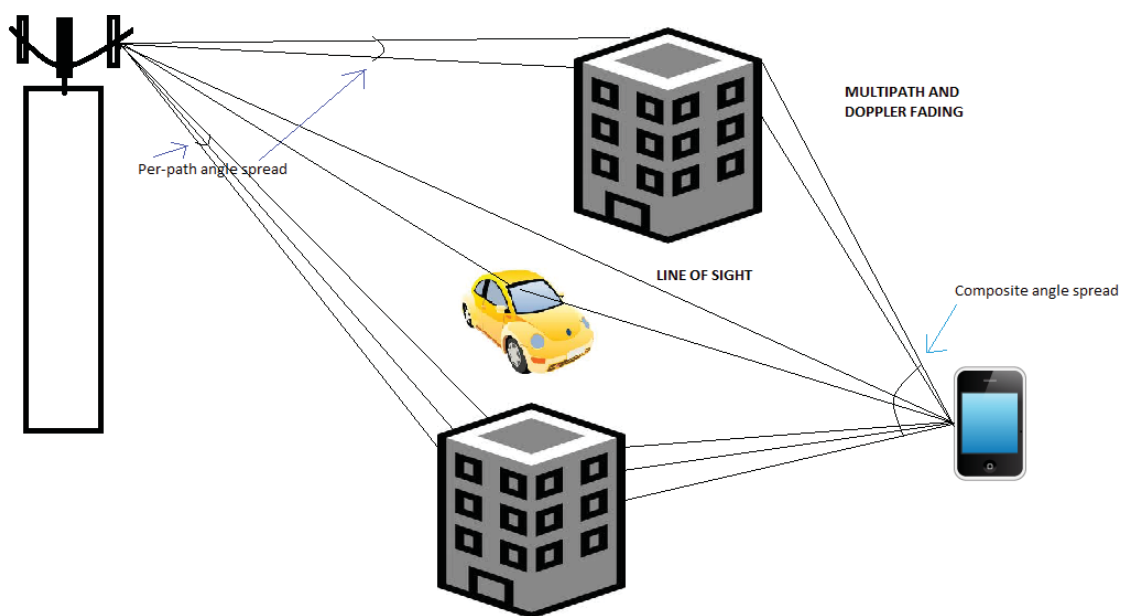


Figure 2.1: A multipath cluster model.

Multipath and Doppler are fundamental phenomena of any wireless channel. Figure 2.1 also illustrates the per-path and composite angle spreads. These are some of the many parameters that are introduced and explained in the subsequent sections.

2.1.1.1 Power Azimuth Spectrum (PAS) and Power Delay Spectrum (PDS)/ Power Delay Profile (PDP)

Consider a uniform linear array (ULA) with an inter-antenna spacing of d , and which receives multiple signal paths each with channel gain α_i , delay τ_i and Angle of Arrival (AoA) ϕ_i . The AoA is defined as the azimuth angle of the incoming path with respect to the broadside of the antenna element [8]. (The array broadside is the direction perpendicular to the array orientation.) As can be seen from Figure 2.2, each path consists of multiple un-resolvable sub-paths (un-resolvable because the difference between the delays of any 2 of these paths is less than the signal sample duration) each arriving at some offset to the mean AoA of the path. The received signal at an antenna element can be expressed as

$$y(t) = \iint h(\phi, t) x(t - \tau) d\tau d\phi + n(t) \quad (3.1)$$

where $h(\phi, t)$ represents the channel as a function of Azimuth-Delay Spread, $x(t)$ is the transmitted signal and $n(t)$ is white Gaussian noise. The instantaneous power azimuth-delay spectrum (PADS) is given as [8]:

$$P_{inst}(\phi, \tau) = \sum_{i=1}^L |\alpha_i|^2 \delta(\phi - \phi_i, \tau - \tau_i) \quad (3.2)$$

where L is the number of paths per antenna element. The average PADS is the average value of the above equation and is formulated as [8]:

$$P(\phi, \tau) = E[P_{inst}(\phi, \tau)] \quad (3.3)$$

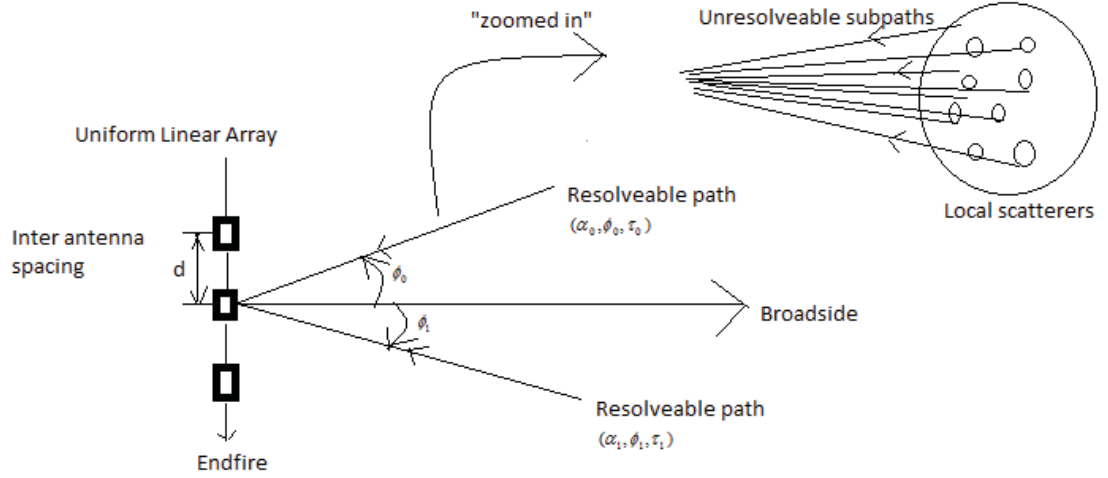


Figure 2.2: Illustration of the multipaths in a multi-antenna setting. $\Delta\phi_m$ is the offset of the m^{th} sub-path from the mean AoA of the corresponding path.

From (3.3) the PAS can be derived by integrating over the delays [8]:

$$P_A(\phi) = \int P(\phi, \tau) d\tau \quad (3.4)$$

As is evident from eq. 3.4 the PAS gives the distribution of the received signal power with respect to the AoAs of the paths. It follows that the PDS/PDP is the distribution of the received signal power with respect to the path delays [8]:

$$P_D(\tau) = \int P(\phi, \tau) d\phi \quad (3.5)$$

Also important are the Angle Spread (AS) and the Delay Spread (DS). The AS is the root mean square (RMS) of angles of an incident path's power at the array [8]:

$$\sigma_A = \sqrt{(\phi - \phi_0)^2 P_A(\phi) d\phi} \quad (3.6)$$

where $\phi_0 = \int \phi P_A(\phi) d\phi$ is the mean AoA. Similarly, the DS is the central moment of the PDS [8] :

$$\sigma_D = \sqrt{(\tau - \tau_0)^2 P_D(\tau) d\tau} \quad (3.7)$$

and $\tau_0 = \int \tau P_D(\tau) d\tau$ is the mean delay.

Shown in Figure 2.3 are typical distributions for the PDS and PAS. The PAS follows a Laplacian distribution although it can also be modeled as uniform. The PDS follows an exponential distribution.

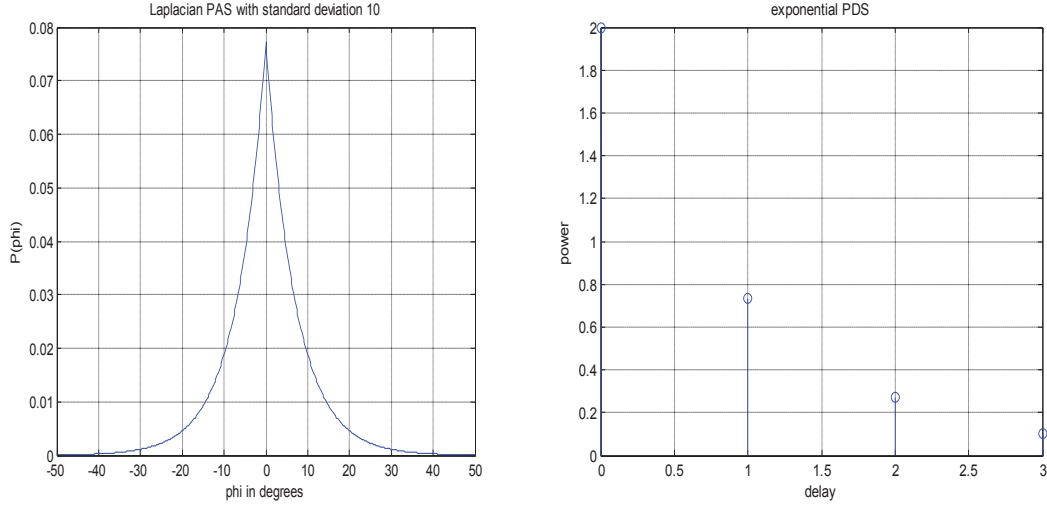


Figure 2.3: Illustration of PAS and PDS.

2.1.2 Spatial Correlation in MIMO arrays

Because of the finite separation between the antenna elements, there exists a correlation between the received signals. Consider 2 antenna elements as shown in fig.

2.4. Let 2 signal rays along a particular path arriving at '1' and '2' at a mean AoA ϕ_0 .

Then they are separated by a path difference $d \sin(\phi_0)$, which is equivalent to a delay of

$(d/c) \sin(\phi_0)$, where c is the speed of light. Let α and β denote the gain and phase of

the path. Assuming a single tap channel, the impulse responses at '1' and '2' can be formulated as [8]:

$$h_1(\phi) = \alpha e^{j\beta} \sqrt{P_A(\phi)} \quad (3.8)$$

$$h_2(\phi) = \alpha e^{j(\beta + 2\pi d \sin(\phi_0) / \lambda)} \sqrt{P_A(\phi)} \quad (3.9)$$

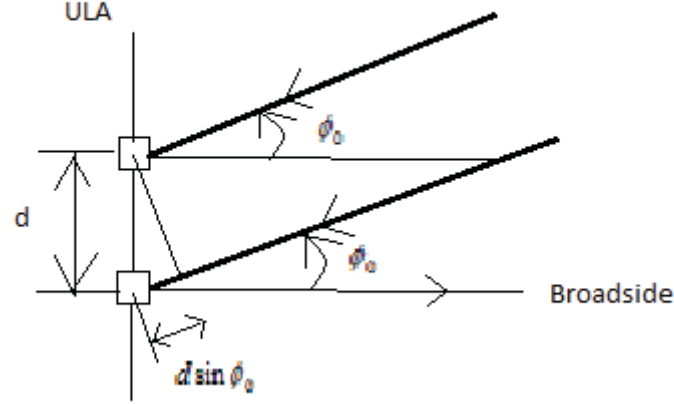


Figure 2.4: Path difference between signals arriving at 2 antenna elements.

The correlation between the received signals as a function of the distance between the antennas and the mean AoA would be given as [8]:

$$\rho(d, \phi_0) = E\{h_1(\phi)h_2^*(\phi)\} \quad (3.10)$$

$$= \int_{-\pi}^{\pi} h_1(\phi)h_2^*(\phi)P_A(\phi - \phi_0)d\phi \quad (3.11)$$

$$= \int_{-\pi}^{\pi} e^{\frac{j2\pi d \sin(\phi - \phi_0)}{\lambda}} P_A(\phi - \phi_0)d\phi \quad (3.12)$$

$$= R_{xx}(d, \phi_0) + jR_{xy}(d, \phi_0) \quad (3.13)$$

where $R_{xx}(d, \phi_0)$ and $R_{xy}(d, \phi_0)$ are the correlations between the real parts and real and imaginary parts of the received signals respectively. Also it has been assumed that the PAS has been normalized. The two terms in (3.12) can be expanded as [8]:

$$R_{xx}(D, \phi_0) = \int_{-\pi}^{\pi} \cos(D \sin(\phi)) P_A(\phi - \phi_0) d\phi \quad (3.14)$$

$$R_{xy}(D, \phi_0) = \int_{-\pi}^{\pi} \sin(D \sin(\phi)) P_A(\phi - \phi_0) d\phi \quad (3.15)$$

where $D = 2\pi d / \lambda$.

Equations (3.14) and (3.15) show that the spatial correlation between 1 and 2 depends on the mean AoA and PAS of the arriving signal as well as the inter-antenna spacing d .

2.1.3 PAS distributions

From empirical measurements it has been shown that the PAS can be modeled in a number of ways. In [9] the PAS was modeled in outdoor scenarios as the n th power of a cosine function. But because of the difficulty in solving the model for correlation functions[10][6], some other models have been introduced. Although the exact distribution depends on the layout of the scatterers, a popular categorization is the uniform distribution for both the BS and MS because of the enormous number of scattered components that arrive at their antennas. The truncated Gaussian and truncated Laplacian distribution are also used, with the latter proposed as the best fit to empirical results in rural and urban areas [6]. The uniform and the truncated Laplacian models are explained in brief below because they have been specified for use in the 3GPP technical document.

2.1.3.1 Uniform PAS model

As is obvious from the name, it is used to model a uniform power distribution over the

specified range of angles. Consider a single 'cluster' of scatterers. The uniform PAS is modeled as [6][8]

$$P_A(\phi) = Q, \quad -\Delta\phi + \phi_0 \leq \phi \leq \phi_0 + \Delta\phi \quad (3.16)$$

The factor Q is derived so as to provide normalization of the received power in the cluster., i.e.[6],

$$\int_{\phi_0 - \Delta\phi}^{\phi_0 + \Delta\phi} Q d\phi = 1 \quad (3.17)$$

Moreover the AS is related to $\Delta\phi$ as $AS = \Delta\phi / \sqrt{3}$.

Substituting (3.16) into (3.14) and (3.15) and simplifying, we get [6][8]

$$R_{xx}(D) = J_0(D) + 4Q \sum_{m=1}^{\infty} J_{2m}(D) \cos(2m\phi_0) \sin(2m\Delta\phi) / 2m \quad (3.18)$$

and

$$R_{xy}(D) = 4Q \sum_{m=1}^{\infty} J_{2m+1}(D) \sin((2m+1)\phi_0) \sin((2m+1)\Delta\phi) / (2m+1) \quad (3.19)$$

where $J_m(\cdot)$ is the m th order Bessel function of the first kind. The envelope correlation coefficient is defined as [8]

$$\rho_e(D) = |R_{xx}(D) + jR_{xy}(D)|^2 \quad (3.20)$$

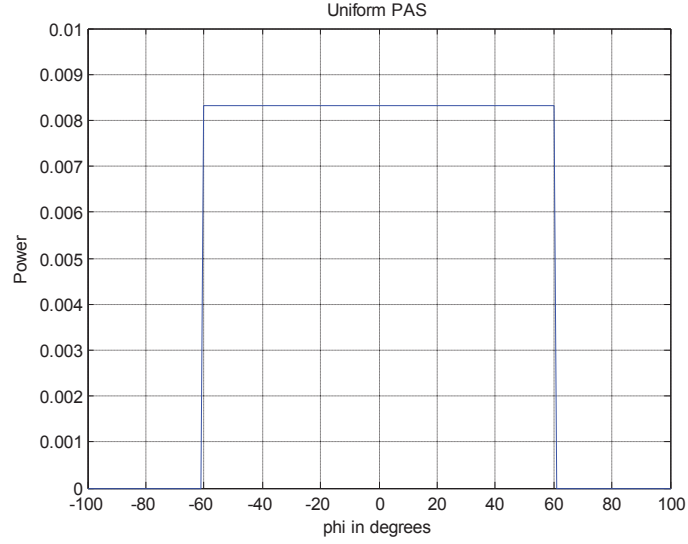


Figure 2.5: Illustration of a uniform PAS with $\phi_0 = 0$ degrees and $\Delta\phi = 60$ degrees.

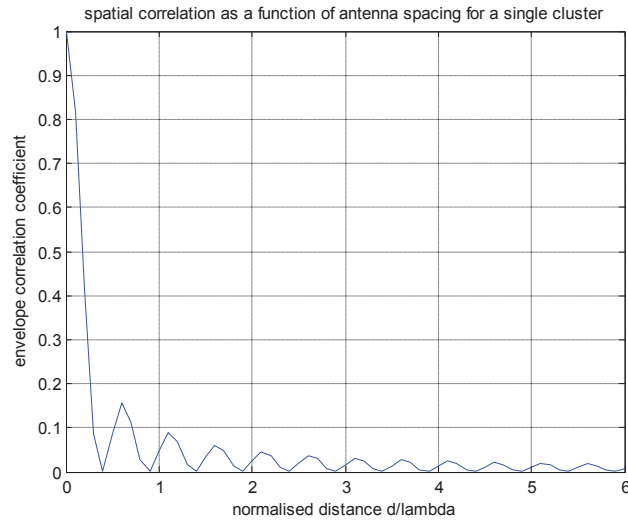


Figure 2.6: The above plot is for an AS of 30 degrees, with $\Delta\phi$ approximated to 60 degrees and $\phi_0 = 0$ degrees.

As can be seen in Figure 2.6, ρ_e decreases with increasing antenna spacing and has periodic zero crossings.

2.1.3.2 Truncated Laplacian PAS model

Consider again a single cluster case. The PAS is modeled as [6][8]

$$P_A(\phi) = \frac{Q}{\sqrt{2}\sigma} e^{-\frac{\sqrt{2}|\phi-\phi_0|}{\sigma}} - \Delta\phi + \phi_0 \leq \phi \leq \phi_0 + \Delta\phi \quad (3.21)$$

where σ is the standard deviation of the PAS. The normalization constant is given by

$$Q \left[1 - e^{-\frac{\sqrt{2}\Delta\phi}{\sigma}} \right] = 1 \quad (3.22)$$

The cross correlation functions are given as:

$$R_{xx}(D) = J_0(D) + 4 \frac{Q}{\sigma\sqrt{2}} \sum_{m=1}^{\infty} J_{2m}(D) \frac{\cos(2m\phi_0)}{\left(\frac{\sqrt{2}}{\sigma}\right)^2 + (2m)^2} \left\{ \frac{\sqrt{2}}{\sigma} + e^{-\frac{\sqrt{2}\Delta\phi}{\sigma}} \left[2m \sin(2m\Delta\phi) - \frac{\sqrt{2}}{\sigma} \cos(2m\Delta\phi) \right] \right\} \quad (3.23)$$

and

$$R_{xy}(D) = 4 \frac{Q}{\sqrt{2}\sigma} \sum_{m=0}^{\infty} \frac{J_{2m+1}(D)}{\left(\frac{\sqrt{2}}{\sigma}\right)^2 + (2m+1)^2} \sin[(2m+1)\phi_0] \left\{ \frac{\sqrt{2}}{\sigma} - e^{-\frac{\sqrt{2}\Delta\phi}{\sigma}} \left\{ (2m+1) \sin[(2m+1)\Delta\phi] + \frac{\sqrt{2}}{\sigma} \cos[(2m+1)\Delta\phi] \right\} \right\} \quad (3.24)$$

2.1.4 Base Station Spatial Parameters [7]

2.1.4.1 BS Antenna Pattern

The technical document [7] specifies a 3-sector/6-sector antenna pattern to be used for each sector. The pattern is specified by:

$$A(\phi) = -\min \left[12 \left(\frac{\phi}{\phi_{3dB}} \right)^2, A_m \right] \quad \text{where } -180 \leq \phi \leq 180 \quad (3.25)$$

ϕ is the angle between the direction of interest and the boresight of the antenna. The

boresight is the direction in which the antenna shows the maximum gain. ϕ_{3dB} is the 3

dB bandwidth and A_m is the maximum attenuation. For the 3 sector case, ϕ_{3dB} is 70 degrees, and $A_m = 20$ dB. The antenna pattern is given in Figure 2.7:

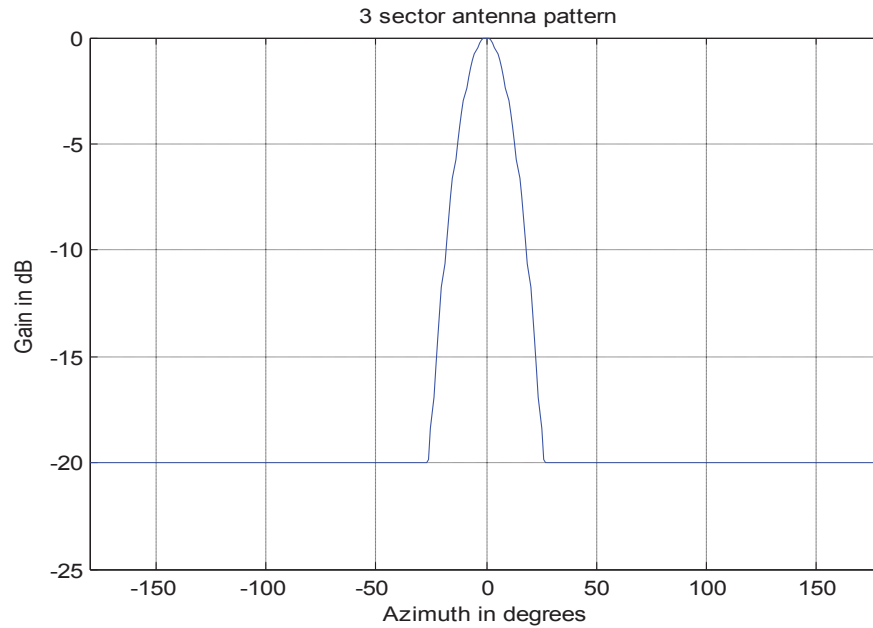


Figure 2.7: Antenna pattern for 3-sector cells.

2.1.4.2 Per-path BS AS

The per-path AS is as already defined above. For the purpose of link level calibration , a concept that will be explained in the next section, the document specifies two values of AS at two different mean angles of departure (AoD) (the model's perspective is for a downlink case).

- AS = 2 degrees at mean AoD = 50 degrees
- AS = 5 degrees at mean AoD = 20 degrees

2.1.4.3 Per-path BS AoD

The AoD is defined as the mean angle with which an arriving or departing path's power

is received or transmitted by the BS array with respect to the boresite. For the purpose of link level calibration, 2 values corresponding to angle spreads mentioned above have been provided in [7]:

- AoD: 50 degrees for an AS of 2 degrees
- AoD: 20 degrees for an AS of 5 degrees

2.1.4.4 Per-path BS PAS

The PAS is assumed to have a Laplacian distribution. However there is a small change to the definition of the PAS here. Because there is some gain associated with the BS antennas, the PAS now is the product of the Laplacian distribution and the BS antenna gain.

$$P(\phi, \sigma, \phi_0) = N_0 \exp\left[\frac{-\sqrt{2} |\phi - \phi_0|}{\sigma}\right] G(\phi) \quad (3.26)$$

where N_0 is the normalization constant as already formulated above. P is the average received power and $G(\phi) = 10^{0.1A(\phi)}$. ϕ represents sub-rays of the path power arriving at an AoD ϕ_0 .

2.1.5 Mobile Station Spatial Parameters [7]

2.1.5.1 MS Antenna pattern

Every antenna element at the MS is assumed to be omnidirectional.

2.1.5.2 Per-path MS AS

As is with the per-path BS AS, two values for the per-path MS AS are considered for calibration:

- AS: 104 degrees resulting from a uniform distribution of PAS over [0,360] deg.
- AS: 35 degrees for a Laplacian PAS with a certain specific AoA.

2.1.5.3 Per-path MS AoA

It is the mean of angles of an incident path's power at the MS with respect to the array broadside. Three different calibration values are considered :

- AoA: -67.5 deg. (for a per-path MS AS of 35 deg.)
- AoA: 67.5 deg. (for a per-path MS AS of 35 deg.)
- AoA: 22.5 deg. (for a per-path MS AS of 35 deg. or with an LOS component)

2.1.5.4 Per-path MS PAS

The per-path MS PAS can be modeled either by the Laplacian model or the Uniform model. The Uniform distribution is taken over a [0 360]deg. Since the antennas are assumed to be omni-directional, no antenna gain is taken into account and the received per-path PAS will remain either Laplacian or Uniform.

$$P(\phi, \sigma, \phi_0) = N_0 \exp \left[\frac{-\sqrt{2} |\phi - \phi_0|}{\sigma} \right] \quad (3.27)$$

2.1.5.5 MS Direction of Travel (DoT)

The mobile station direction of travel is defined with respect to the broadside of the MS array.

2.1.5.6 Per-path Doppler Spectrum

The per-path Doppler spectrum is formulated as a function of the per-path MS PAS, MS DoT and AoA.

2.2 Scope of the Ray Tracing Model

The model specifies two methods of operation: link level calibration mode and system level simulation mode. Since the model is based on the summing of signal rays arriving at particular angles with respect to the broadside of the antenna array, it is but a snapshot of the channel. Moreover the MS is moving at a particular velocity as a result of which the angles will evolve with time as the position of the mobile changes. Since each snapshot of the channel produces a particular set of channel coefficients, this is a computationally intensive process as a function of time. Because of the snapshot nature, this model can be used for both calibrating the user's algorithm as well as for running system level simulations that can be used for comparing the performance of different algorithms and accounting for system attributes such as scheduling and HARQ. Towards this end, parameters for calibration are provided in the report, including various PDSs with specific values of powers and delays, mobile velocities and DoTs, BS and MS PASs and AoDs/AoAs.

System level simulations are described, as is the case with link level simulations, in the context of a downlink case, with reciprocity in the uplink. The major difference between a link level and system level simulation is that while the former consists of a single BS transmitting to a single MS, the latter aims to obtain performance metrics such as throughput and delay by -

- simulating over multiple sectors/cells, BSs and MSs.

- running simulations over multiple drops. A drop is basically a simulation run for a finite number of cells/sectors, BSs, MSs and over a specified number of data frames.

The convention is to keep the cell layout and the locations of the BSs fixed over a series of 'D' drops while the MSs are randomly re-positioned at the beginning of each drop.

Thus the result of the spatial channel model (SCM) for a P-element BS array and an Q-element MS array is an Q-by-P matrix of complex amplitudes for each of the multi-paths that is a function of time because of the movement of the mobile. It is therefore inferred that the MS undergoes fast fading within a drop.

The literature [7] suggests a few different well established scenarios for use in the channel generation. These include the suburban and urban macro cell case (about 3 km inter BS spacing) and the urban micro cell case (about 1 km inter BS spacing). The latter is different from the other two in that a LOS component is considered, the angle spread at the BS is larger and different paths are shadowed differently. The basic steps suggested in generating the channel are selection of the scenario, determining the user parameters and then generating the channel coefficients. The user parameters include:

- Angles of departure and angles of arrival.
- Path powers
- Path delays
- Mobile velocity vector
- Antenna gains and path loss
- Shadow fading and Rice K-factor

- Antenna spacing
- Per-path PAS, per-path angle spread and sub-path phase offsets

The model described in the literature [7] generates the angular parameters, the path powers and the path delays as random variables using defined probability density functions depending on the scenario. But the implementation in this thesis leaves the definition of these parameters to the user. But certain other scenario-specific parameters such as the angle spreads at the BS and MS, and path loss models are retained to broadly reflect the environment. For example, when an LOS component exists and a K-factor is given, the sub-path offsets are automatically chosen according to a 5 degree AS rather than a 2 degree AS to reflect a microcell environment as against a macrocell environment.

2.3 The Spatial Snapshot of the Channel

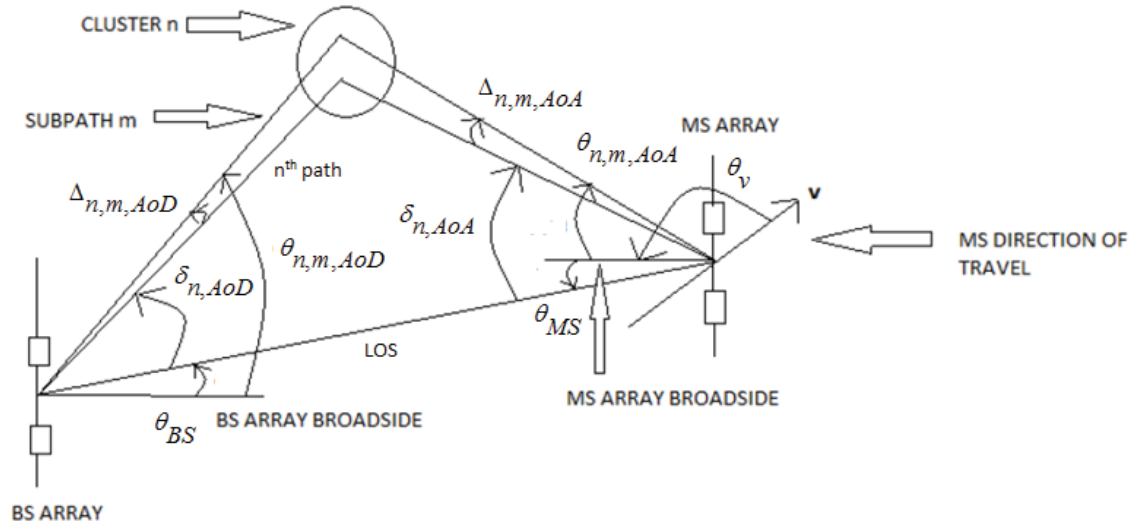


Figure 2.8: Illustration of the fundamental angular parameters of the SCM.

Figure 2.8 illustrates the important angular parameters used in channel generation [7]:

- θ_{BS} : LOS AoD direction between the BS and MS with respect to broadside of BS array.
- $\delta_{n,AoD}$: AoD of the n th path ($n=1 \dots N$) with respect to the LOS AoD.
- $\Delta_{n,m,AoD}$: Offset of the m th path ($m=1 \dots M$) sub-path of the n th path with respect to $\delta_{n,AoD}$.
- $\theta_{n,m,AoD}$: Absolute AoD for the m th path sub-path of the n th path at the BS with respect to BS broadside.
- θ_{MS} : Angle between the BS and MS LOS path and the MS broadside.
- $\delta_{n,AoA}$: AoA for the n th path ($n=1 \dots N$) with respect to the LOS AoA.
- $\Delta_{n,m,AoA}$: Offset of the m th sub-path of the n th path with respect to $\delta_{n,AoA}$.
- $\theta_{n,m,AoA}$: Absolute AoA for the m th sub-path of the n th path at the MS with respect to the BS broadside.
- v : MS velocity vector.
- θ_v : Angle of the velocity vector with respect to the MS broadside.

By convention the angles measured in a clockwise direction are taken to be negative in value. These parameters are used in the channel generation formula explained in the next section. Before that, some important assumptions needed for the system level simulations need to be outlined:

- 1) The mobile experiences fast fading in each path in every drop as mentioned earlier. But there are certain parameters that are kept constant *during* a drop. These include the angle spread, delay spread, log normal shadowing and the MS location.
- 2) The AoD/AoA values are identical for the uplink and downlink.
- 3) Although the performance simulation here is done only for a single mobile, the literature advises that when considering multiple mobiles, shadowing among them in uncorrelated.

- 4) The antenna configuration could be generic. Reference antenna spacings of 0.5λ , 4λ and 10λ are used.
- 5) As can be inferred from Figure 2.8, the elevation spread is not modeled.
- 6) The maximum number of resolvable paths modeled is 6 with 20 sub-paths each for all scenarios. The number of paths is decided keeping in mind that the system bandwidth is approximately 5MHz.

Although the first assumption talks about the fading behavior being evolved in time within a drop, the MS location is changed only at the *beginning* of each drop. Thus there is no variation of the angular parameters within a drop as the mobile moves. Therefore there seems a need for some enhancement of the current model with respect to this aspect. This is precisely what [11] has proposed. This extension of the 3GPP SCM named Spatial Channel Model Extended (SCME) proposes a number of enhancements to the current model including:

- Extension of the bandwidth of operation from 5 MHz in the 2 GHz band to 100 MHz in both the 2 and 5 GHz bands.
- Introduction of drifting of tap delays and angles of arrival with the mobile movement within a drop.
- LOS for all scenarios.
- Changes in the path loss models for use in the 5 GHz band.

Only the drifting of angles of arrival has been taken into account in this thesis for use in the system level simulations. Since the changes in the tap delays are quite small

and less than a sample duration, and since the path delays in this work are implemented in terms of the system's sample duration, this modification is not considered.

2.4 Generation of channel coefficients

Consider an S-element linear BS array and a U-element linear MS array. The channel coefficients for the n th multipath component are given by a U-by-S matrix of complex amplitudes, where each element can be expressed as [8]:

$$h_{u,s,n}(t) = \sqrt{nthPathPower} \sum_{m=1}^M \left\{ \left(\sqrt{\frac{BS}{PAS}} \right) \begin{pmatrix} Phase \\ due \\ to \\ BSarray \end{pmatrix} \left(\sqrt{\frac{MS}{PAS}} \right) \begin{pmatrix} Phase \\ due \\ to \\ MSarray \end{pmatrix} \begin{pmatrix} Phase \\ due \\ to \\ Doppler \end{pmatrix} \right\} \quad (3.28)$$

where M is the number of sub-paths per path. Now, as mentioned earlier, the BS PAS is taken to have a Laplacian distribution and the MS PAS can be either Laplacian or uniform over $[0,360]$ degrees. Thus the problem of power allocation for these M subpaths is now a straightforward application of the distribution. But next comes the question of how the angles, or rather the offsets from the mean AoD/AoA of the n th path are chosen for these sub-paths. Thus it is a question of how the PAS is now sampled for the subpaths. Two approaches have been considered by the SCM Ad-Hoc Group of 3GPP: the uniform power subpath method and the sampled Laplacian method.

With the uniform power subpath method, the offset angles are allocated by ensuring that the areas of the different sections of the PAS divided by the sub-rays are equal (equal areas = equal powers). Consider a Laplacian PAS $P(\phi, \sigma)$ with a mean AoA

of 0 degrees. Let there be 2 sub-rays in each path. Now the area between the 2 subpaths, distinguished by their offset angles ϕ_1 and ϕ_2 , is [8]:

$$\int_{\phi_1}^{\phi_2} P(\phi, \sigma) = -\frac{1}{2} \left(e^{-\frac{\sqrt{2}|\phi_2|}{\sigma}} - e^{-\frac{\sqrt{2}|\phi_1|}{\sigma}} \right) \quad (3.29)$$

$$= \frac{1}{\alpha(M+1)} \quad (3.30)$$

where α is a normalization factor. There exist different scenarios for α and M:

- $\alpha = 1$ if M is odd.
- $\alpha = 2$ for the 2 symmetric angles with the smallest absolute value and $\alpha = 1$ for all other subpaths, if M is even.

In the case of the 2 sub paths, (3.30) takes the value 6. The offset angle with the same power is found as [8]

$$\phi_{m+1} = -\frac{\sigma}{\sqrt{2}} \left[\ln \left(e^{-\frac{\sqrt{2}\phi_m}{\sigma}} - \frac{2}{\alpha(M+1)} \right) \right] \quad m = 0, 1, 2, \dots, \lfloor M/2 \rfloor - 1 \text{ and } \phi_0 = 0 \text{ deg.} \quad (3.31)$$

If M is even, ϕ_1 is found by setting $\phi_0 = 0$ but no subpath is allocated at 0 degrees. When M is odd, there exists one subpath at $\phi_0 = 0$. In both these cases, all the other offsets are calculated according to (3.31). The other M/2 subpaths are at the mirrored negative offsets.

Therefore, under the uniform power subpath [7], (3.28) is expressed as:

$$h_{u,s,n}(t) = \sqrt{\frac{P_n \sigma_{SF}}{M}} \sum_{m=1}^M \left(\begin{aligned} & \sqrt{G_{BS}(\theta_{n,m,AoD})} \exp(j[kd_s \sin(\theta_{n,m,AoD}) + \Phi_{n,m}]) \times \\ & \sqrt{G_{MS}(\theta_{n,m,AoA})} \exp(jkd_u \sin(\theta_{n,m,AoA})) \times \\ & \exp(jk\|\mathbf{v}\| \cos(\theta_{n,m,AoA} - \theta_v) t) \end{aligned} \right) \quad (3.32)$$

where P_n is the power of the n th path, σ_{SF} is the standard deviation of shadow fading applied as a bulk parameter to all the paths, k is the wave number $2\pi/\lambda$, d_s and d_u are the distances in meters from BS antenna element s and MS antenna element u respectively from the respective reference antenna elements, $\Phi_{n,m}$ is the phase of the m th subpath of the n th path, $\|\mathbf{v}\|$ is the magnitude of the MS velocity and θ_v is the angle of the MS velocity vector.

In the sampled Laplacian method, the powers of the subpaths follow a Laplacian PAS while the offsets are distributed asymmetrically around the average AoA. There is a two step procedure to the determination of the offsets [8]:

1. M reference offsets are generated by allocating them uniformly over the range $[-\alpha, \alpha]$. α varies with the given angular spread.
2. Next the actual offsets corresponding to the subpaths are generated by adding an arbitrary random number between $[-0.5, 0.5]$:

$$\phi_m = -\alpha + m\delta + \kappa \text{ where } \kappa \text{ is a uniform random number over } [-0.5, 0.5]$$

and $\delta = 2\alpha / M$. (3.28) can now be written as [8],

$$h_{u,s,n}(t) = \sqrt{P_n \sigma_{SF}} \sum_{m=1}^M \left(\begin{aligned} & \sqrt{G_{BS}(\theta_{n,m,AoD}) P_{BS}(\theta_{n,m,AoD})} \exp(j[kd_s \sin(\theta_{n,m,AoD}) + \Phi_{n,m}]) \times \\ & \sqrt{G_{MS}(\theta_{n,m,AoA}) P_{MS}(\theta_{n,m,AoA})} \exp(jkd_u \sin(\theta_{n,m,AoA})) \times \\ & \exp(jk\|\mathbf{v}\| \cos(\theta_{n,m,AoA} - \theta_v) t) \end{aligned} \right) \quad (3.33)$$

In the presence of an LOS component, the channel coefficients of (3.32) can be broken down as [7]:

$$h_{u,s,n=1}^{LOS}(t) = \sigma_{SF} \sqrt{\frac{K}{K+1}} \left(\frac{\sqrt{G_{BS}(\theta_{BS})} \exp(j[kd_s \sin(\theta_{BS})]) \times \sqrt{G_{MS}(\theta_{MS})} \exp(j[kd_u \sin(\theta_{MS}) + \phi_{LOS}])}{\exp(jk\|\mathbf{v}\| \cos(\theta_{MS} - \theta_v)t)} \right) + \sqrt{\frac{1}{K+1}} h_{u,s,1}(t) \quad (3.34)$$

and for $n \neq 1$:

$$h_{u,s,n}^{LOS}(t) = \sqrt{\frac{1}{K+1}} h_{u,s,n}(t) \quad (3.35)$$

where θ_{BS} is the AoD for the LOS component at the BS, θ_{MS} is the AoA for the LOS component at the MS and ϕ_{LOS} is the phase of the LOS component. K is the Rice K-factor. Only one sub-ray in the first path is subject to LOS.

Chapter 3

LabVIEW Implementation of the channel model

3.1 Overview

The implementation of the ray tracing MIMO channel model was done in LabVIEW Professional Development System Version 11.0. It consists of a handful of blocks/virtual instruments (VI) that have been designed to mimic a hardware based real-time emulator as closely as possible:

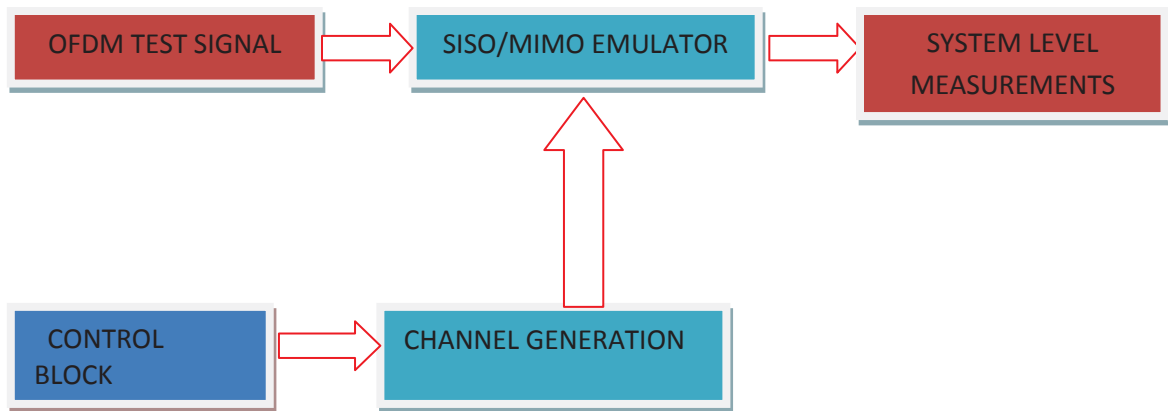


Figure 3.1: Overview of the LabVIEW system implementation blocks.

1. **CONTROL BLOCK** : The control block is the controller of the channel generation VI. All the inputs needed to generate a set of channel coefficients starting from the antenna profile to the velocity of the mobile are provided through the implementation of this VI. It is a simple user interface. Some portions of the interface are shown below:

Calibration (on) or Simulation (off)

channel type for simulations
Fading+AWGN

Control for simulations
Manually enter parameters

Channel PDP for calibration mode
Modified Pedestrian A LOS

Tx antennas
0

Rx antennas
0

Path-Loss

BS antenna height (in m)
0

MS antenna height (in m)
0

Carrier frequency (in Mhz)
0

Distance between BS and MS (d) (in m)
calibration uses the first value. simulation uses the array.
0 0

Path loss model
suburb

Path information

Theta BS, angle of BS array broadside with LOS direction
0

Angles of Departure (AoD's) for the N paths
0 0 0 0 0 0 0 0

Theta MS, angle of MS array broadside with LOS direction
0

Angles of Arrival (AoA's) for the N paths
0 0 0 0 0 0 0 0

Ricean K factor in linear units
0

LOS phase
0

Figure 3.2: A partial snapshot of the control block user interface.

2. **CHANNEL GENERATION:** This is responsible for the generation of the channel coefficients and operates for both the calibration and the simulation mode. In the calibration mode, 4 PDPs are supported while these have to be manually provided by the user in the (system level) simulation mode. Since there is no concept of a drop in the calibration mode, the channel is a matrix for each of the N multipaths.

In the simulation mode, there are N matrices for every drop.

3. **SISO/MIMO EMULATOR:** This VI is a tapped delay line implementation of the convolution operation of the channel. There are separate VIs for the SISO and MIMO cases. In addition, there is the optional implementation of a transmit/ receive diversity system as well.

Because the tapped delay lines have to be manually set up and wired and because the delays can be arbitrary for the system simulation mode, the number of delay blocks have been limited to 15 multiples of the input sample rate. For the calibration mode, which run on various predefined PDPs this is not an issue.

4. **OFDM TEST SIGNAL:** Here, the OFDM test signal is generated for an M-QAM system. It takes a number of inputs such as the size of the QAM constellation, the size of the FFT, the number of symbols to generate and outputs the OFDM sequence with a CP attached to each symbol.

5. **SYSTEM LEVEL MEASUREMENTS:** This VI is responsible for evaluating the effect of the channel on the OFDM input by computing the BER for various scenarios such as different PDPs, presence or absence of diversity schemes, and variation of the

model's parameters. These are discussed in more detail in the next chapter on performance evaluation.

3.2 LabVIEW Virtual Instruments (VIs)

LabVIEW is a graphical programming language. Unlike traditional procedural programming which follows a sequential flow of execution in a code, the execution in LabVIEW depends on the flow of wires between different 'blocks'. This enables parallel processing of the LabVIEW code. The LabVIEW code is basically an implementation of a traditional 'text-based' code in the form of execution blocks (VIs) and wires that interconnect these VIs. These VIs can be pre-defined, user-defined or a combination of both. There are a bunch of in-built/pre-defined VIs that are used as the basis for building any VI. For example, array operations like array indexing, random number generation, signal mapping etc. are all pre-defined in LabVIEW as graphical blocks. Any number of user-defined VIs can be joined together in a logically correct manner to form a bigger VI. In this case, the smaller VIs are called sub-VIs. This ensures that code once 'drawn' can be re-used.

In Figure 3.1, the control block is just an interface that accepts system and channel parameters from the user. In LabVIEW terminology, it is a 'cluster' of different types of values. As illustrated by Figure 3.2, these values include an array of double-precision floating point values for the angles, K-factor, LOS phase, antenna heights and frequency of operation, numeric constants for the number of Tx/Rx antennas, and string constants for path loss model and channel PDP. Selection of the calibration or

simulation mode is done using a binary switch. Thus a cluster is similar to a structure in C. This cluster is passed as data to the channel generation VI. This is similar to passing values between different modules of a C program. The channel generation VI uses these parameters to generate the channel coefficients using (3.32), (3.34) and (3.35) and generates an output cluster of its own. This cluster contains among other things, the complex coefficients, tap delays, mobile velocity, coherence time and the number of samples per coherence time, and is then passed to the emulator VI. This VI also has two case structures for supporting the calibration and simulation modes. The major difference between the two is that the calibration case supports the default power delay profiles as sub-cases while the simulation mode accepts all inputs from the user. Snapshots of the channel VI can be found in the Appendix B.

The OFDM VI uses the FFT size and the number of OFDM frames as input to generate the sub-carriers. There is an in-built (pre-defined) VI to perform the FFT operation. When repetition codes are employed, symbol repetition is performed accordingly before IFFT. The output cluster of this VI consists of the complex OFDM output and its size. Appendix C illustrates the OFDM VI.

The SISO/MIMO emulator VI take as inputs the OFDM test signal cluster, channel output cluster and another cluster from the control block that includes the number of Tx/Rx antennas, the number of paths and the mode of operation. It performs convolution of the input with the channel using a tapped-delay line. The delay, multiplication and accumulation operation are placed inside a timed loop that does exactly the same operation as a 'for' loop in C with the exception that the loop executes

at the specified rate. This rate is the input sample rate. This can be set up using the loop-input options of the timed loop and ensures real-time operation. The output of the emulator is a complex signal point every $(1/\text{input sample rate})$ seconds for every receiver antenna. This output is accumulated over the length of the input block and then passed to the system-measurement VI. Also, as many timed loops are employed as there are sub-channels in the system: 4 for 2 x 2 MIMO and 1 for SISO.

In the actual implementation, the OFDM, channel and emulator VIs are placed as sub-VIs in the system emulator VI. Here, the average bit error rate is calculated over the specified number of iterations for various values of E_b/N_0 . The receiver assumes perfect channel knowledge and performs maximum ratio-combining when diversity/beamforming or repetition codes are employed. Otherwise it just performs zero-forcing on the received signal. The error values are then exported to MATLAB for plotting. MATLAB is used since it provides easy and convenient options for editing the plots. Appendices D and E further illustrate the emulator and system-measurements VIs.

3.3 The National Instruments Real-Time System

Owing to the real-time requirements of the channel emulation, the SISO/MIMO emulator block cannot be implemented on any host PC as the operating systems (OS) on these machines are not suited for real-time applications. This is because of the simple and basic reason that these are general purpose OS and there is no *guarantee* that the scheduled task will be completed within the imposed timing constraint. A real-time

system is an information processing system which has to respond to external events both correctly and within a finite, specified time [12]. Thus the correctness and usefulness of the system depends not only on the logical results of its computations, but also on the time at which they are produced. Here the timing impositions are made by the input sample rate. The SISO/MIMO emulator has to be able to accept the OFDM input at a specified sample rate consistently and perform the operations of delay, multiplication and addition correctly.

Figure 3.3 shows the real-time development tools of National Instruments. There are three components to a National Instruments real-time system [13]:

1. **Host computer with LabVIEW:** This is the computer on which LabVIEW is installed and all the VIs described above are developed. These VIs can be downloaded and run on RT targets.
2. **RT Target :** An RT Target is a piece of hardware that runs the RT Engine and VIs created on the host computer. It communicates with the host using an Ethernet cable.
3. **RT Engine:** It is a version of LabVIEW that runs on RT targets. It provides real-time deterministic performance for the following reasons:
 - It runs on a real-time operation system (RTOS) such as the Ardence Phar Lap ETS or the Wind River Vx Works.
 - RT targets are designed to run only the VIs and device drivers necessary for RT applications, which prevents other applications from impeding the execution of RT VIs.

- RT targets do not use virtual memory because of its unpredictable performance.

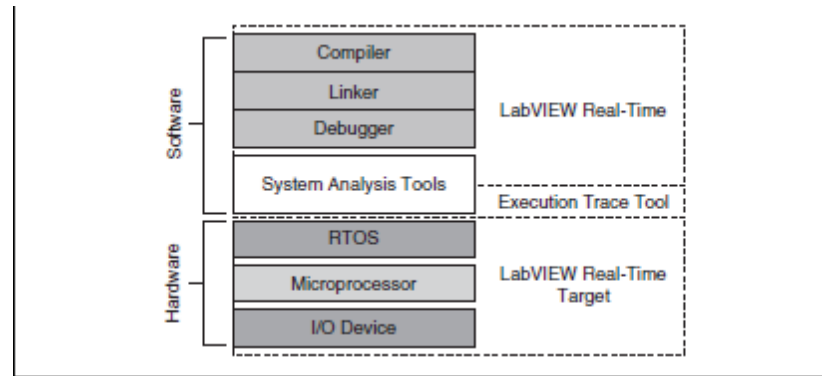


Figure 3.3: Real-time development tools [13].

In Chapter 1, it was mentioned that only the emulation operation has to be done in real time and that the channel generation can be done offline on a PC, implying that the emulation is done on high speed hardware. But for a software implementation such as in this thesis, this translates to assigning *priorities* to the two operations as these run on the same real-time platform. This is the crux of the real-time module of the National Instruments package.

The emulator VI consists of single/multiple 'timed loops' performing the tapped delay line convolution. These timed loops are like the traditional 'for' loops of C but are executed at the specified rate. These loops would therefore ideally run at the inverse of the system bandwidth. But there is a physical constraint with regard to the maximum clock speed on the RT system and this is just 1 MHz. Therefore, the actual rate of the loops is $\min(1\text{MHz}, \text{system bandwidth})$. Since the channel emulator in this thesis is

based on 3GPP standards, these bandwidths are in the range of 7.68 Mhz. This necessitates the need to scale down the whole system. Thus, sample rates and the path delays all have to be scaled down and scaled up, respectively. The detailed numbers are produced in the performance analysis section.

Time critical VIs and timed loops inside them are responsible for running the time critical section of the VI codebase. Since all the VIs are deployed onto the real-time system and since the Control VI, the Channel Generation VI and the Systems Evaluation VI are not time critical, they are assigned a 'normal' priority. This is the default priority.

The set of priorities for VIs in increasing order are:

- Background priority (lowest)
- Normal priority (default)
- Above normal priority
- High priority
- Time-critical priority (highest)

A time-critical priority preempts all other priorities. A VI with such a priority does not relinquish processor resources until it completes all tasks. Timed loops execute at a priority below the time-critical priority of any VI but above high priority. Thus, now the emulator VIs are placed in the highest time critical priority compared to the system evaluation VI, as these can run after the entire emulation process is finished. A comprehensive block diagram is now in order:

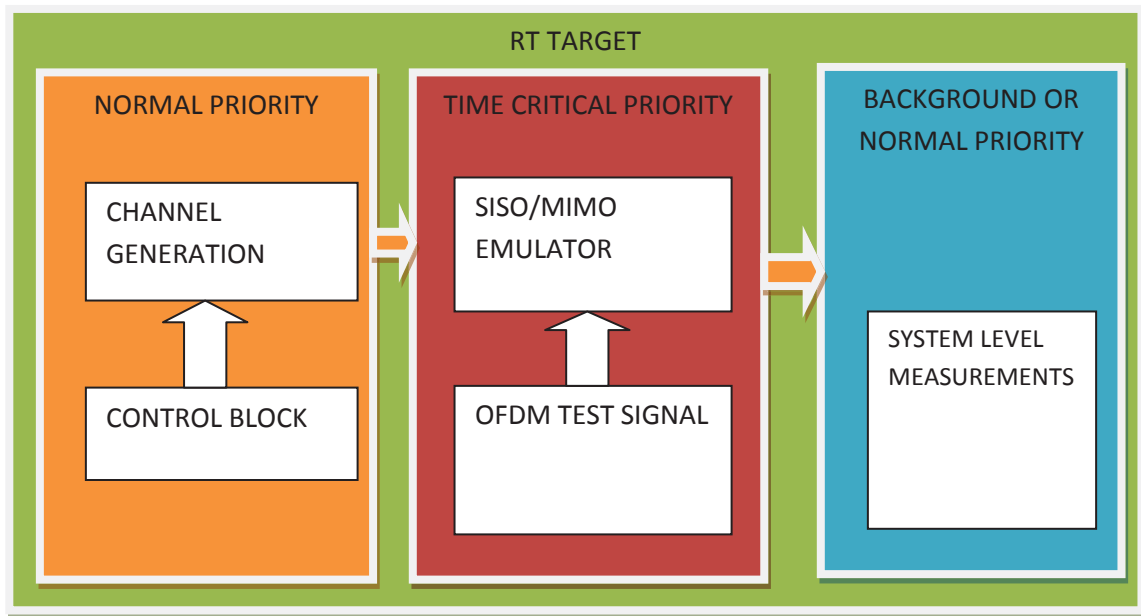


Figure 3.4: Illustration of the system implementation inside the RT platform.

Chapter 4

Simulations and Performance Evaluation

4.1 Purpose of the simulations

Now that the channel has been constructed with the help of a plethora of parameters, the next obvious step is to mould it into representing the scenario that we wish to emulate, and then tweak the parameters to see how they affect the input. Thus it is the validation step of the channel model.

A whole host of parameters have been considered to make these system level simulations cover a wide range of possible scenarios. Tables 4.1 and 4.2 list them.

Transmission Parameters	Value(s)
System Bandwidth	960 KHz (scaled down from 7.68 MHz)
Number of OFDM subcarriers	128
Sub-carrier spacing	7.5 KHz
Cyclic Prefix	32
Iterations	1000
Antenna Profiles	2 x 2, 1 x 1 (considered for performance evaluations) 1 x 2, 2 x 1 (optional)
Frame size	3
Base stations/mobile stations	1/1
SNR range	[-15,30]dB
Diversity scheme for SISO	(1,4) and (1,8) Repetition codes

Diversity scheme for MIMO	MRC using symbol repetition at Tx; Beamforming using CSI at the Tx
Frequency of operation	1900 MHz

Table 4.1: A summary of the transmission parameters.

The system bandwidth has been down scaled from 7.68MHz to 960 KHz to fit within the maximum clock speed of the real-time system which is 1MHz.

Channel Parameters	Value(s)
Max. Resolvable Paths	6
Subpaths/path	20
Angle spreads at BS	2° , 5°
Angle spread at MS	35°
PAS at BS	Laplacian with uniform power subpath allocation
PAS at MS	Laplacian with uniform power subpath allocation
Antenna spacing at MS	0.5λ
Antenna spacing at BS	0.5λ , 4λ , 10λ
K factor	6dB
Antenna pattern	3 sector
Power Delay Profiles	ITU Modified Pedestrian A w/ and w/o LOS ITU Vehicular A ITU Pedestrian B
Shadow Fading	8 dB - NLOS cases 4 dB - LOS case
Path Loss Models	COST231 Hata Urban Propagation Model COST231 Walkfish-Ikegami street canyon model - for LOS

Table 4.2: A summary of the channel parameters.

The path delays in the ITU channel models are scaled upwards by a factor of 8 and have properties as listed in Table 4.3:

PDP	Paths	RMS Delay Spread (musec. ²)	Max. Relative Delay	Mobile Velocities (kph)	Coherence Time (sec.)	Coherence Bandwidth
Modified Pedestrian A LOS on	5	0.188	3	3	0.08	1.06MHz
Modified Pedestrian A LOS off	4	0.403	3	30/120	0.008/0.002	495 KHz
Vehicular A	6	2.72	19	3/30/120	0.08/0.008/0.002	73.3 KHz
Pedestrian B	6	4.85	28	3/30/120	0.08/0.008/0.002	41.6KHz

Table 4.3: Parameters of the ITU PDPs.

4.2 Simulation Results

4.2.1 SISO

The SISO channel is generated as a special case of the general MIMO formula eqn. 3.32.

Here the MS is taken to be omni-directional with a gain of 0dB. Path loss is not included in the channel generation step. The following graphs show the results of the SISO channel for the modified pedestrian LOS off, vehicular and pedestrian profiles.

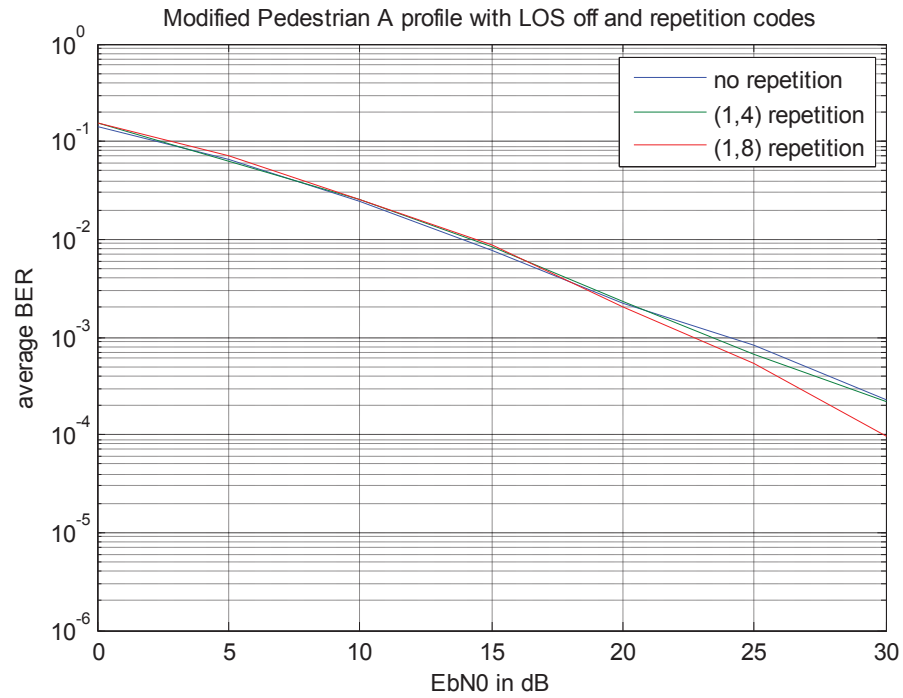


Figure 4.1: BER for the modified pedestrian A profile with LOS off.

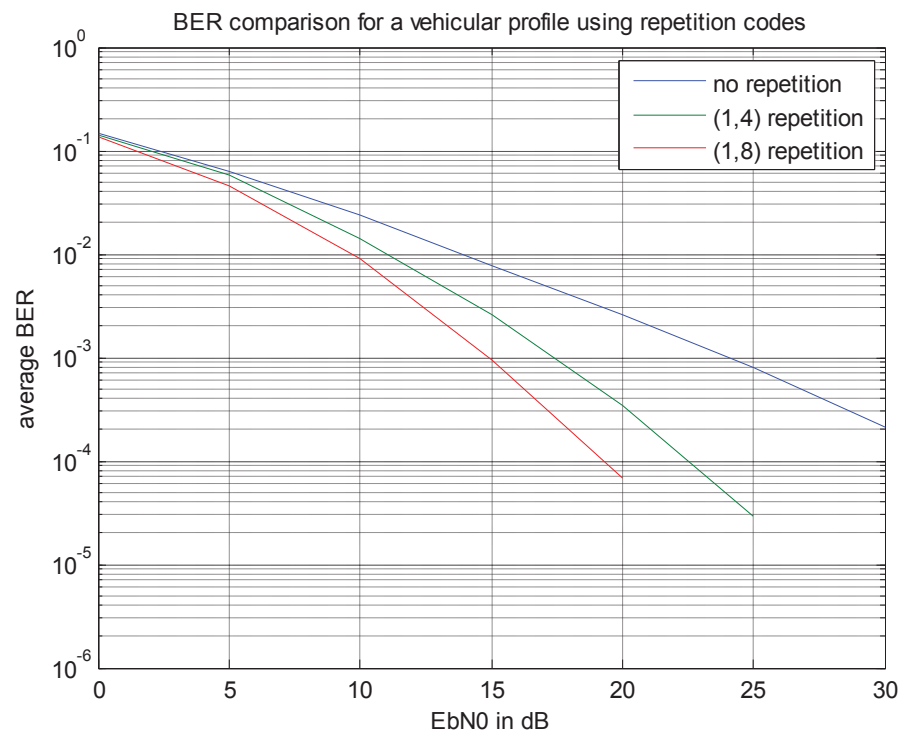


Figure 4.2: BER for the vehicular A profile.

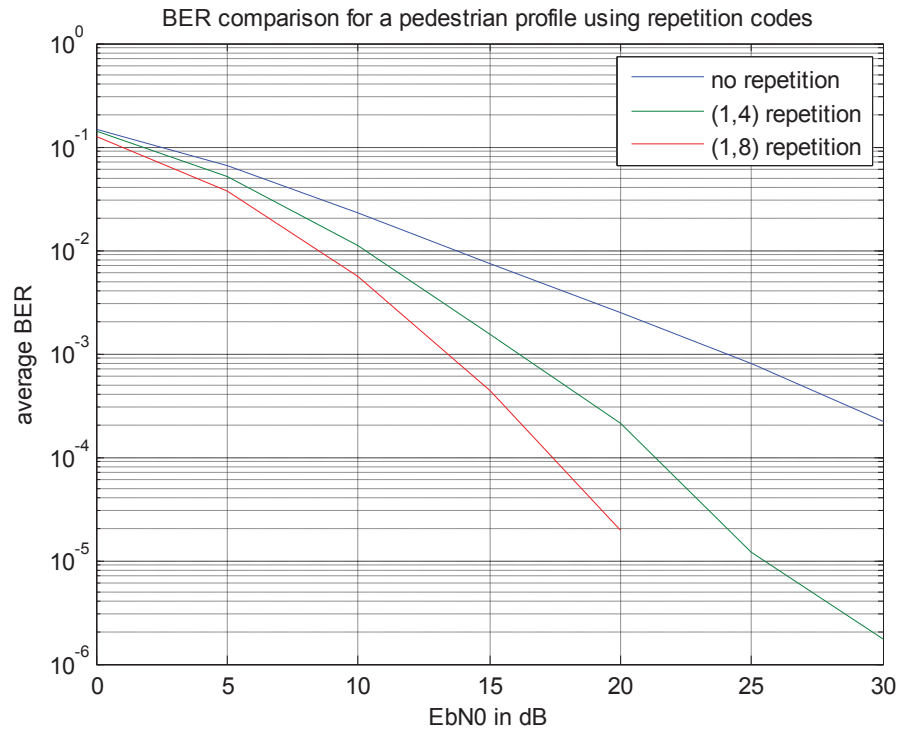


Figure 4.3: BER for the pedestrian B profile.

Figures 4.1, 4.2 and 4.3 suggest the case that the modified pedestrian profile is the least frequency selective of all the three cases, which is indeed correct as can be verified from Table 4.3.

4.2.2 2 x 2 MIMO

The MIMO case allows us to vary a whole range of parameters and observe the effects on the input. These include the antenna spacing, angle spread, K factor, mean AoA, diversity and beamforming. In all these cases, the path loss is included in the channel generation step by multiplying it as a bulk parameter with every coefficient in the channel matrix. The MS is taken to be omni-directional with a gain of 0 dB.

Fig. 4.5 illustrates the average BER performance of OFDM for the modified pedestrian profile for varying inter antenna spacing at the BS, for a 3 sector case. Since correlation between the antenna elements increases the error rate in a fading environment and since spatial correlation increases with decreasing antenna spacing, 10λ has the best error curve of the three values.

Figure 4.6 plots the BER curve for a single tap channel for varying mean AoA at the MS. An illustration of the situation is given in figure 4.4. A 90-degree AoD implies the wavefronts of any path are along the endfire of the antenna and hence there is maximum path difference between the waves arriving at the different elements. For an AoD of 0 degrees, the wavefronts are along the broadside of the array and there is zero phase difference between them. Hence the correlation is also minimum and the error rate is higher for the larger mean AoA case.

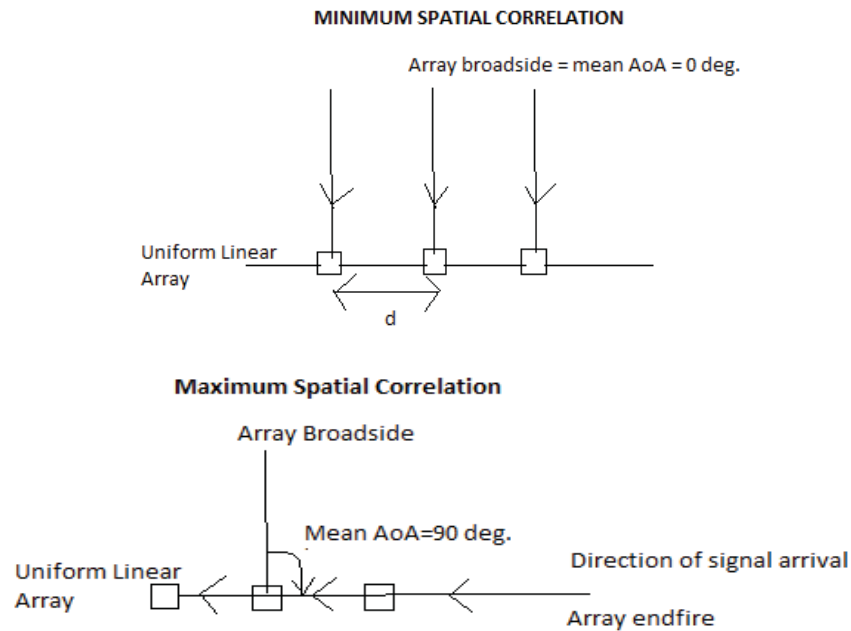


Figure 4.4: Illustration of the dependence of spatial correlation on mean AoA.

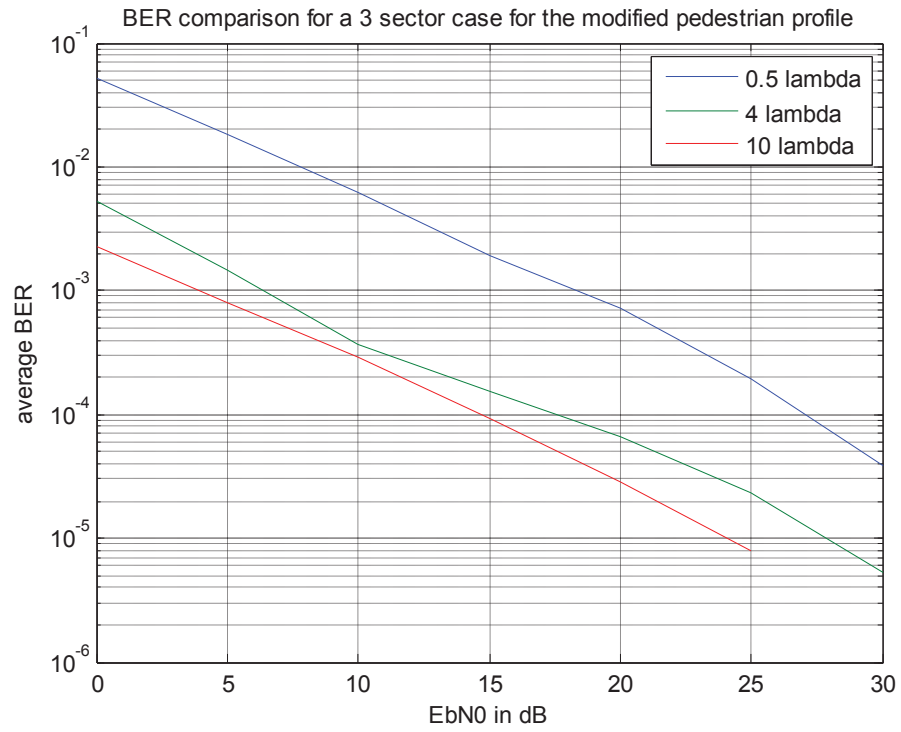


Figure 4.5: BER for the NLOS modified pedestrian profile for varying antenna spacing at the BS.

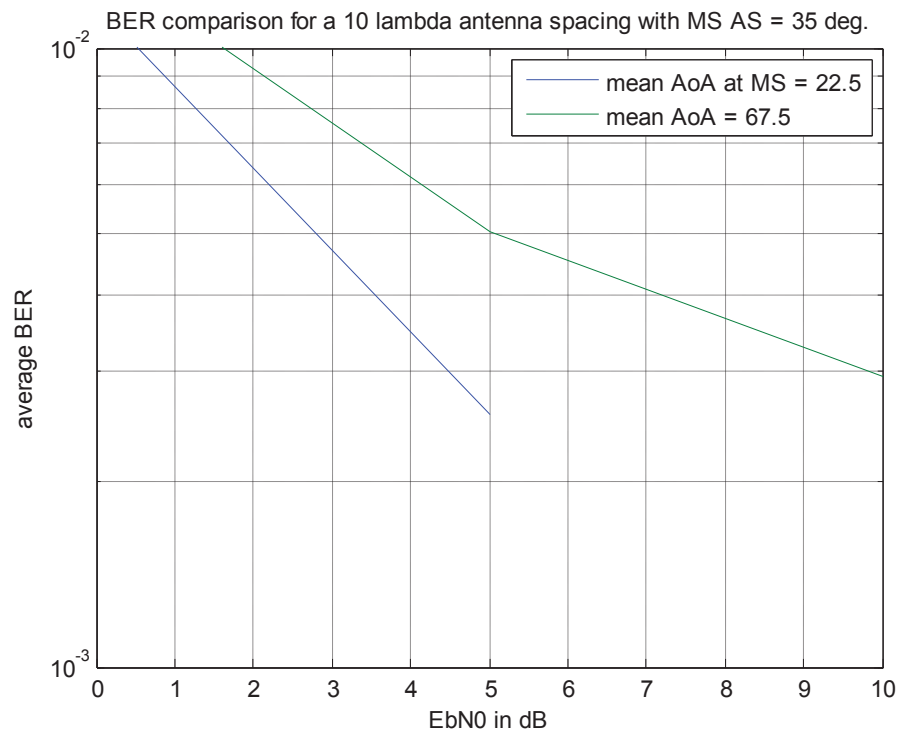


Figure 4.6: BER for a single tap channel for varying mean AoA.

Figures 4.7, 4.8 and 4.9 show the BER as a function of varying antenna spacing but for a spatial diversity scheme. Here the same symbol is transmitted from both the Tx antennas, one being the complex conjugate of the other, and at the receiver an MRC strategy is employed. Thus the bad performance with a small antenna spacing can be improved to at least an order of magnitude with spatial diversity.

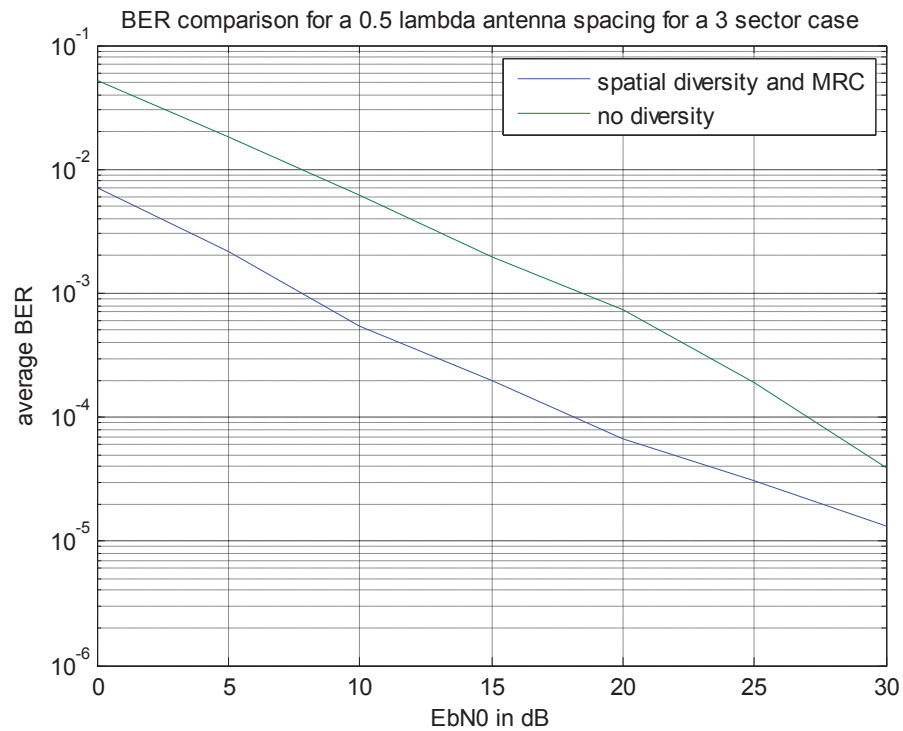


Figure 4.7: BER for a spatial diversity scheme for an antenna spacing of 0.5λ in a 3 sector case.

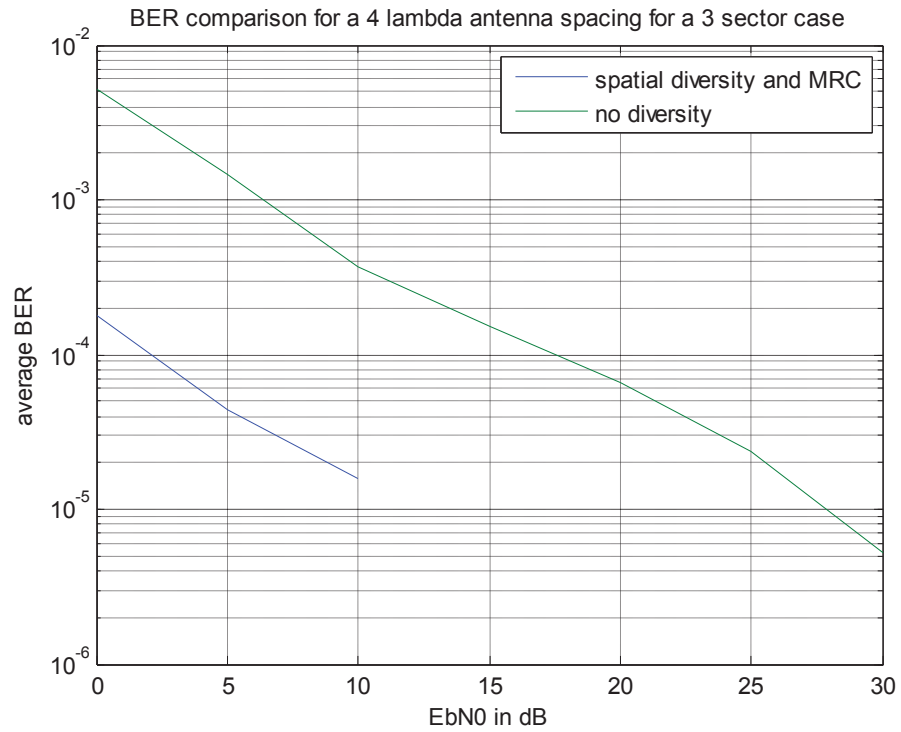


Figure 4.8: BER for a spatial diversity scheme for an antenna spacing of 4λ in a 3 sector case.

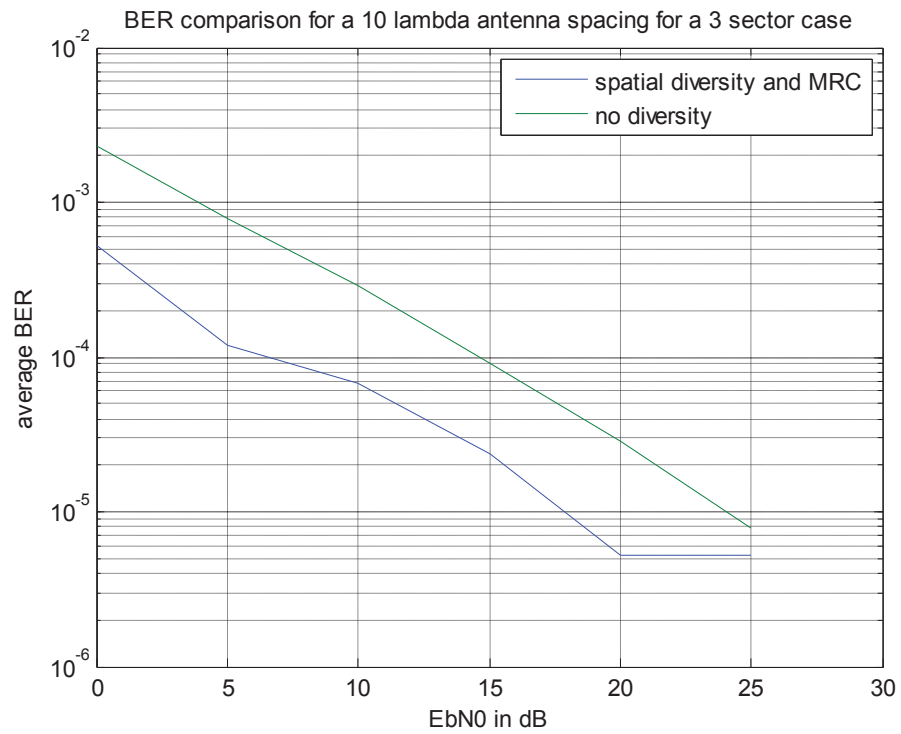


Figure 4.9: BER for a spatial diversity scheme for an antenna spacing of 10λ in a 3 sector case.

Figure 4.10 shows the error rates when beamforming is employed at the BS with the assumption of knowledge of the CSI. Beamforming is effected through singular value decomposition (SVD) of the channel. Every transmit symbol is repeated in the 2 Tx antennas.

Beamforming with CSI knowledge at the Tx gives a much bigger diversity gain than the straightforward MRC at the receiver as can be seen in the figures. The performance for any given antenna spacing can be at least 2 orders of magnitude higher. This is therefore a more attractive BER-ameliorating scheme for small antenna spacings of 0.5λ and 4λ .

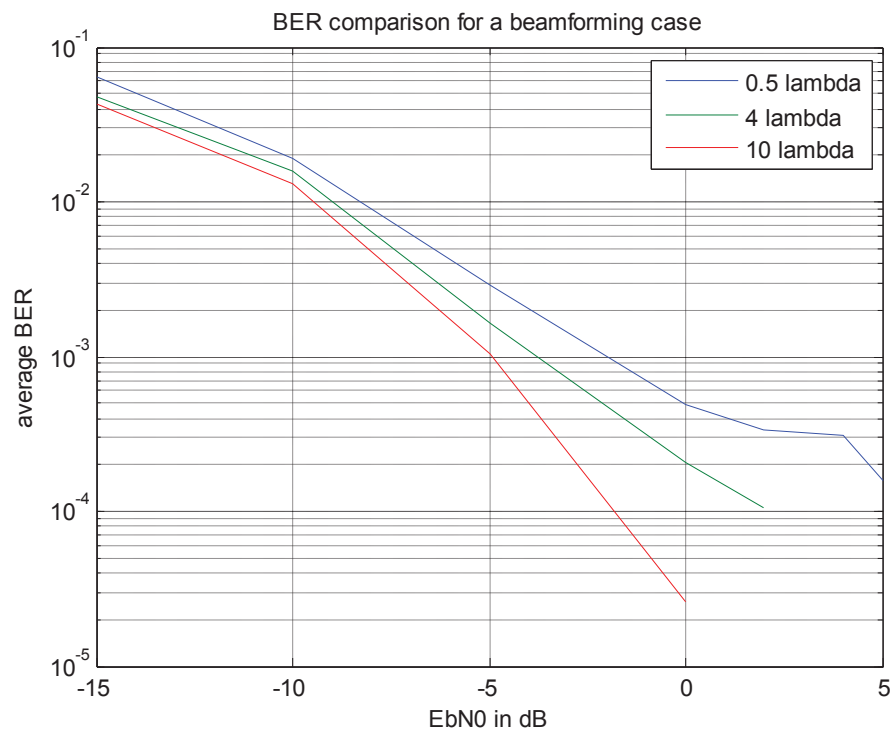


Figure 4.10: BER for a beamforming MIMO system for 0.5 lambda antenna spacing.

Figures 4.11 and 4.12 illustrate the spatial correlation between the BS antennas for 2 values of angle spread. In Figure 4.11, for an angle spread of 2 degrees, it can be seen that the correlation is higher for higher values of mean AoD, for the same reason explained above for Figure 4.6.

Figure 4.12 illustrates the same case for an AS of 5 degrees. A higher per-path AS performs better for a similar reason. For an AoD of, say, 90 degrees, a higher AS implies a smaller phase difference between the subpaths at the adjacent antenna elements. Therefore the correlation is also minimum. In fact, (3.12) for the spatial correlation between 2 antenna elements can be written as [8]:

$$\rho(d) = \frac{1}{M} \sum_{m=1}^M e^{\frac{j2\pi d \sin \theta_{n,m,AoA}}{\lambda}} \quad (4.1)$$

where the integral has been replaced by a summation over 20 subpaths for the uniform power subpath allocation strategy.

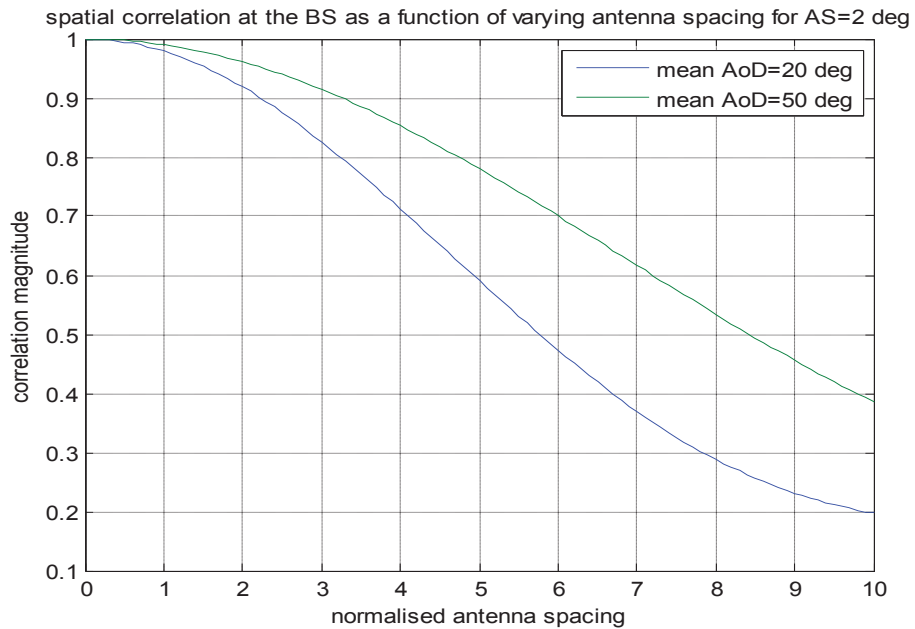


Figure 4.11: Spatial correlation at the BS as a function of varying antenna spacing for AS= 2 deg.

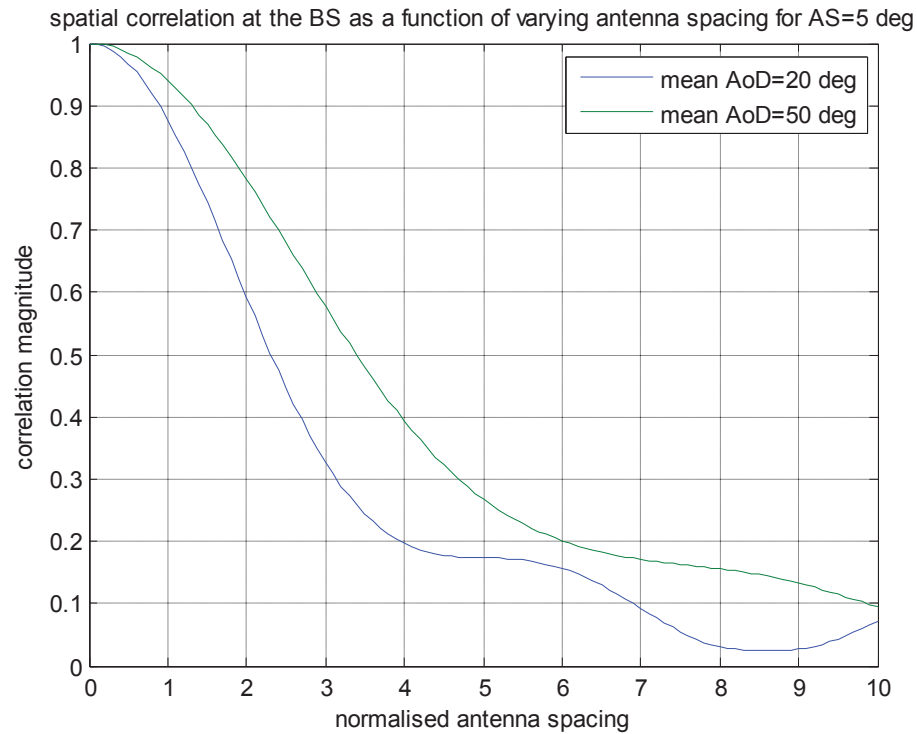


Figure 4.12: Spatial correlation at the BS as a function of varying antenna spacing for AS= 5 deg.

Figures 4.13, 4.14 and 4.15 show the spatial correlation at the BS now as a function of varying mean AoD. Firstly, it is obviously understood that a smaller antenna spacing causes higher correlation. Secondly this correlation is periodic. It rises to maximum at 90 degrees and then drops off to zero at 0 degrees for the exact reason illustrated in the previous 2 graphs. Between Figures 4.13 and 4.14 correlation for the latter is higher because of the smaller AS.

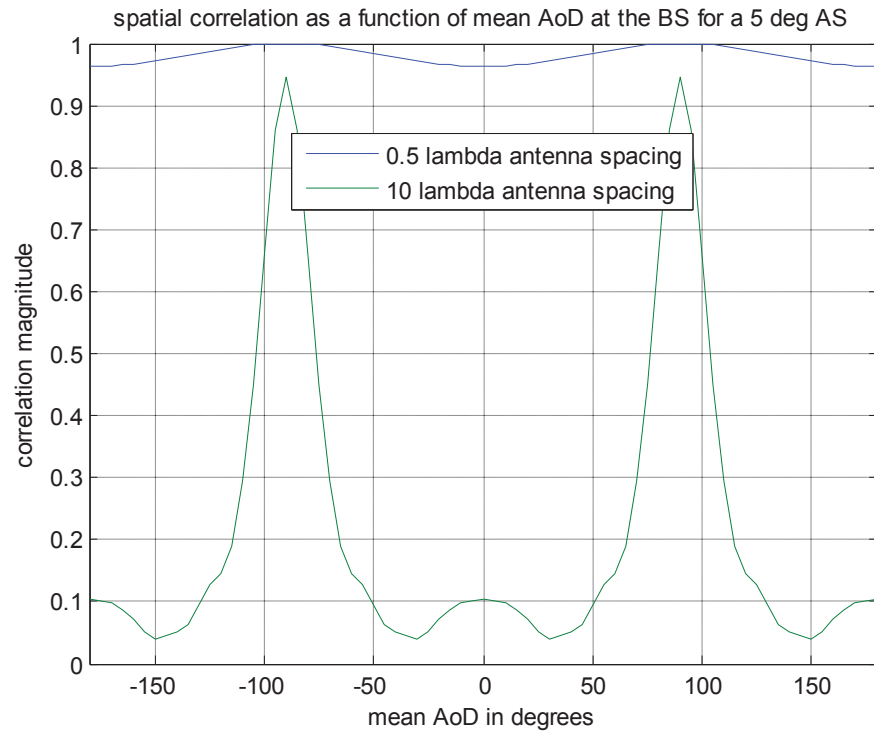


Figure 4.13: Spatial correlation at the BS as a function of varying AoD for AS=5 deg.

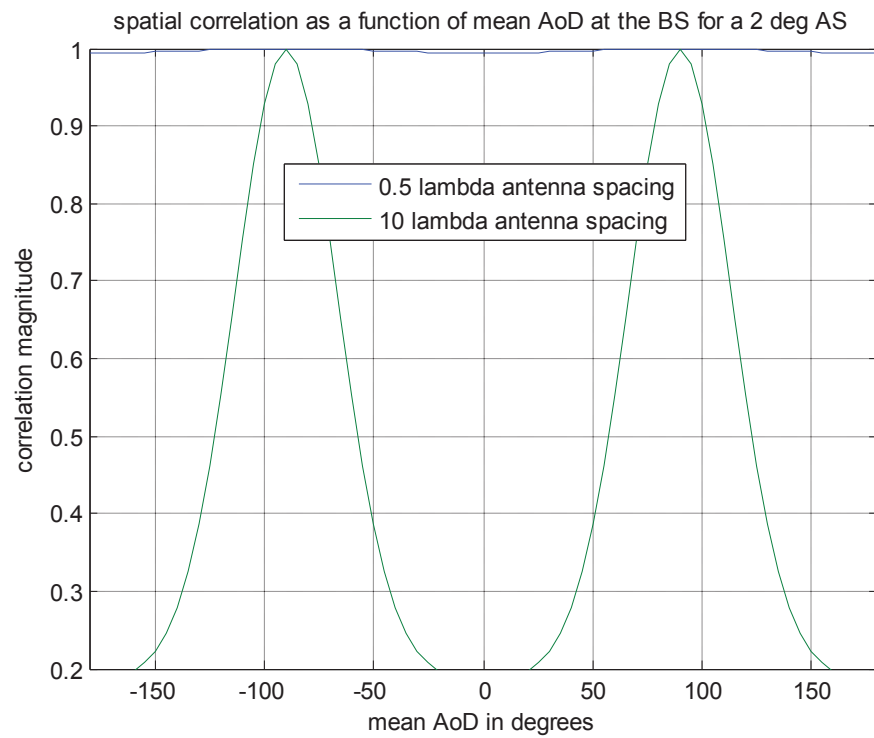


Figure 4.14: Spatial correlation at the BS as a function of varying AoD for AS=2 deg.

Figure 4.15 is a zoomed in version of the 0.5λ case in fig. 4.15.

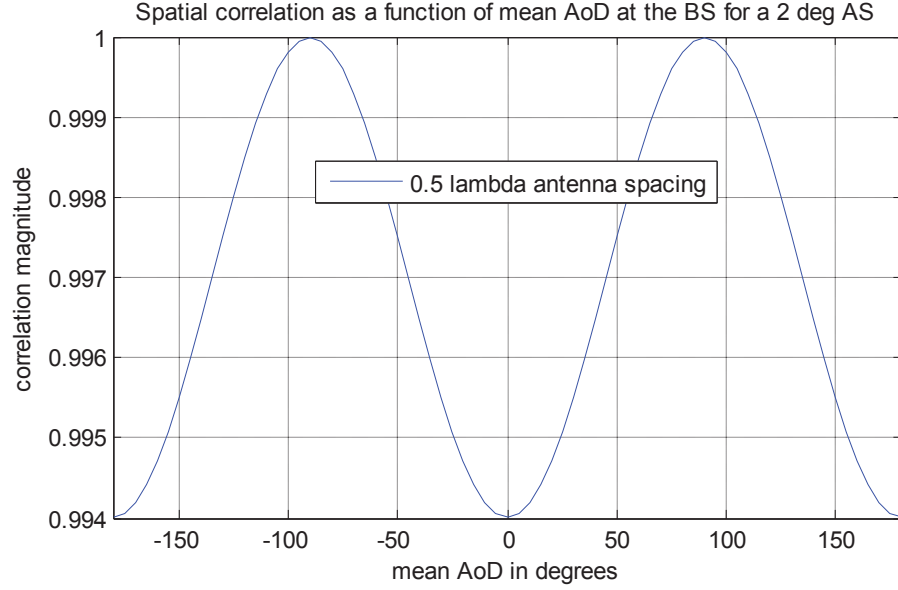


Fig. 4.15: Spatial correlation at the BS as a function of varying AoD for 0.5 lambda inter antenna spacing.

Figure 4.16 shows the temporal correlation between the antenna elements at the MS as a function of the normalised distance traveled. Here the phase difference between the antenna elements depends not on the AoA but on the difference between the AoA and the direction of travel as this gives the angle between the propagating waves and the mobile. If this difference is 0 degrees, it means the wavefronts are along the endfire of the antenna array and so the correlation is maximum. If the difference is 90 degrees it means the wavefronts are along the broadside of the array and the correlation is minimum. It is also clear mathematically from the following expression [8]:

$$\rho(\tau) = E\{h_{s,u,n}(t+\tau) \cdot h_{s,u,n}^*(t)\} \quad (4.2)$$

$$= \frac{1}{M} \sum_{m=1}^M e^{\frac{j2\pi v \cos(\theta_{n,m,AoA} - \theta_v)}{\lambda}} \quad (4.3)$$

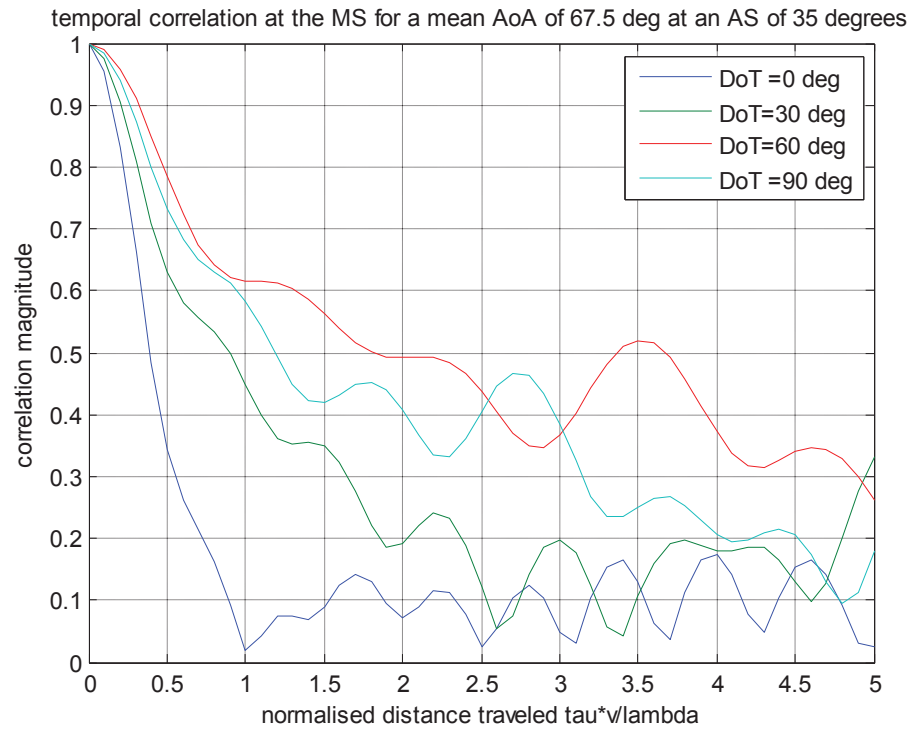


Figure 4.16: Temporal correlation at the MS for varying distance traveled.

Chapter 5

Conclusions and future work

This thesis focused on developing a MIMO channel emulator that can be run on a real-time system. After discussing its need, the general methodology for channel emulation was investigated following which candidates for channel models were briefly introduced. The reasons for choosing the ray tracing model were enumerated following which the structure of the model and its scope were explained in detail. The various parameters that go into the model were defined and understood and the formula for generating the channel coefficients was given. Next, the implementation details in LabVIEW were delved into. Specifically the overall block diagram of the emulation operation was presented and the real-time capabilities/limitations of LabVIEW and National Instruments hardware were discussed. This helped to adapt the block diagrams for running on the real-time system. Finally the process of channel validation was begun by simulating the SISO channel for various power delay profiles and diversity schemes and passing an OFDM test signal through it and observing the BER curves for accuracy. The major tests were done by varying the parameters that induce spatial correlation among the antennas, including the antenna spacing, angle spread and the antenna beamwidth. The K factor was also changed to observe its effects on the input. These were embedded into diversity and beamforming techniques to check how these could be used to reinforce/mitigate the effects caused by the parameters. The spatial and

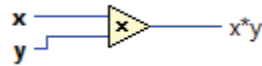
temporal correlations of the model were also plotted and understood, thus helping to gain an in-depth knowledge of the ray tracing channel model.

Potential future work consists of deploying the emulator to hardware to make it truly real-time. This also alleviates the bandwidth constraints posed by the clock speed limitation of the real-time system as the sampling at the hardware DACs and ADCs happen at a higher rate.

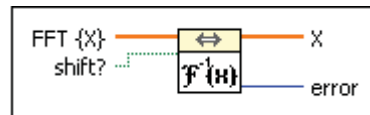
APPENDIX A

Examples of VIs used in the implementation:

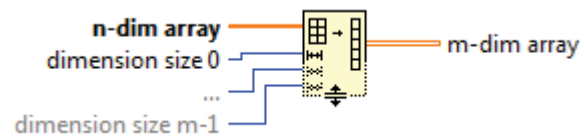
- Arithmetic VI - multiplication



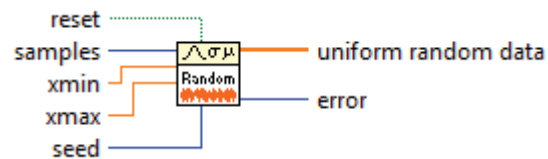
- Signal Processing VI - IFFT:



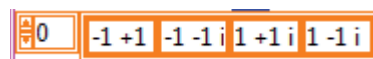
- Array Processing VI - Reshaping an n-dim array to an m-dim array:



- Uniform Random number generator:



Example of an array declaration:

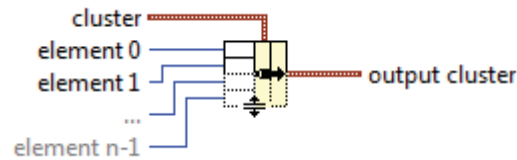


A 'For' loop:



N is the number of times the loop has to run. 'i' is the loop index.

Building a cluster from individual values:



Numerical Controls and Indicators:

Double precision floating point Control

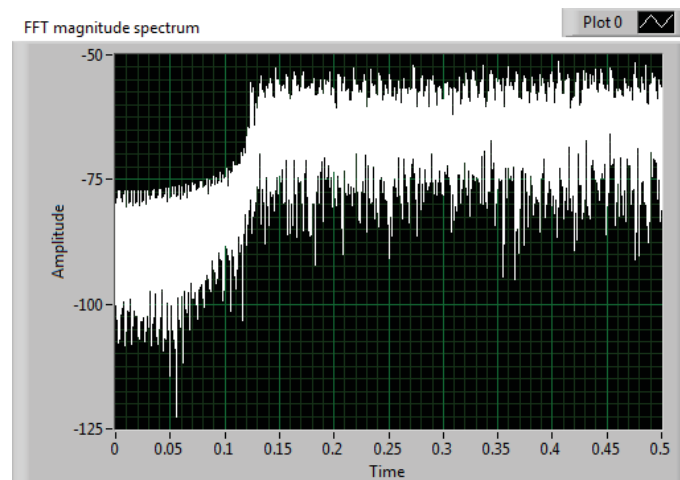


Double precision floating point Indicator

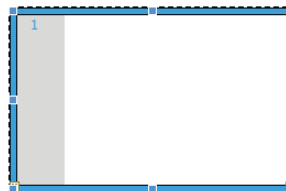


Controls and indicators are similar to user variables for input and output respectively.

Example of a Graphical indicator:



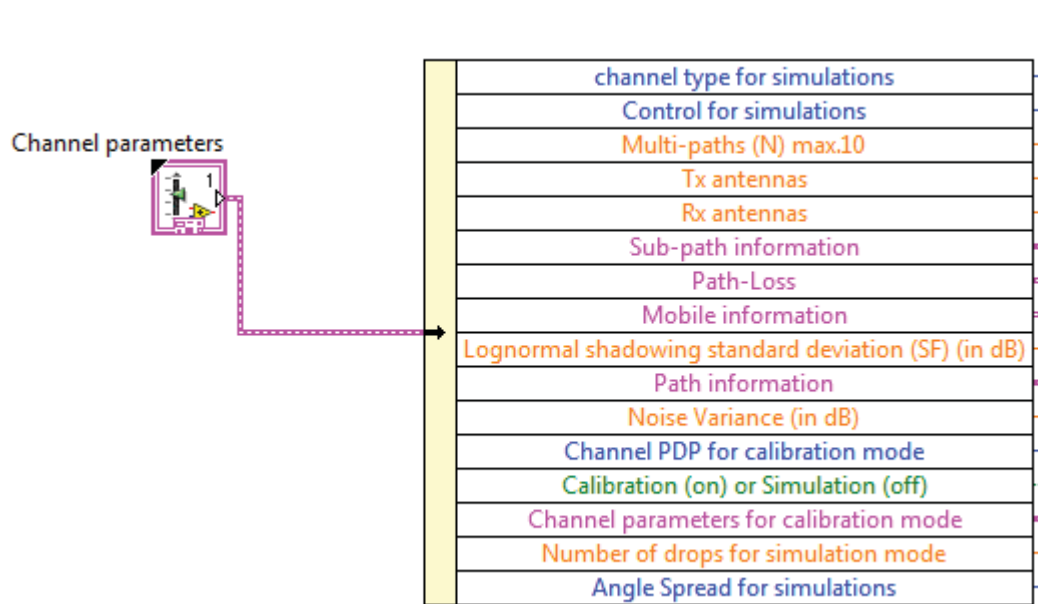
MathScript NODE:



A MathScript node executes LabVIEW MathScripts and other text-based scripts using the MathScript RT Module engine. It is used in the LabVIEW implementation when complex formulae involving a large number of arithmetic operations have to be put together.

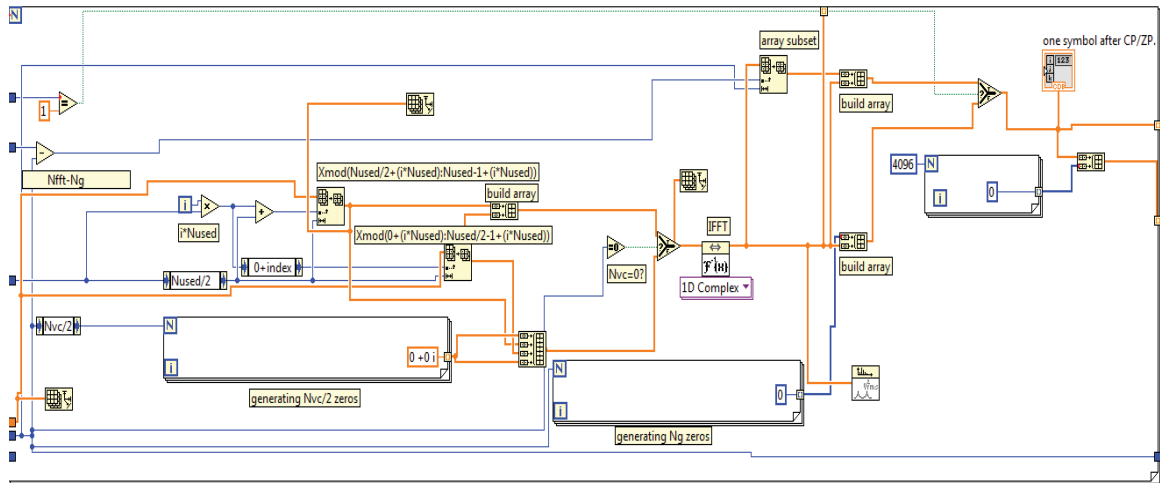
APPENDIX B

Channel Parameters cluster and its elements:



The 'Channel parameters' cluster is 'unbundled' to give the individual elements. It is the basically just an instance of the control block. Here the elements in blue represent string constants, green elements are binary valued, pink elements are sub-clusters and orange elements are floating-point values. All these values are then used to generate the channel coefficients using the equations in chapter 2.

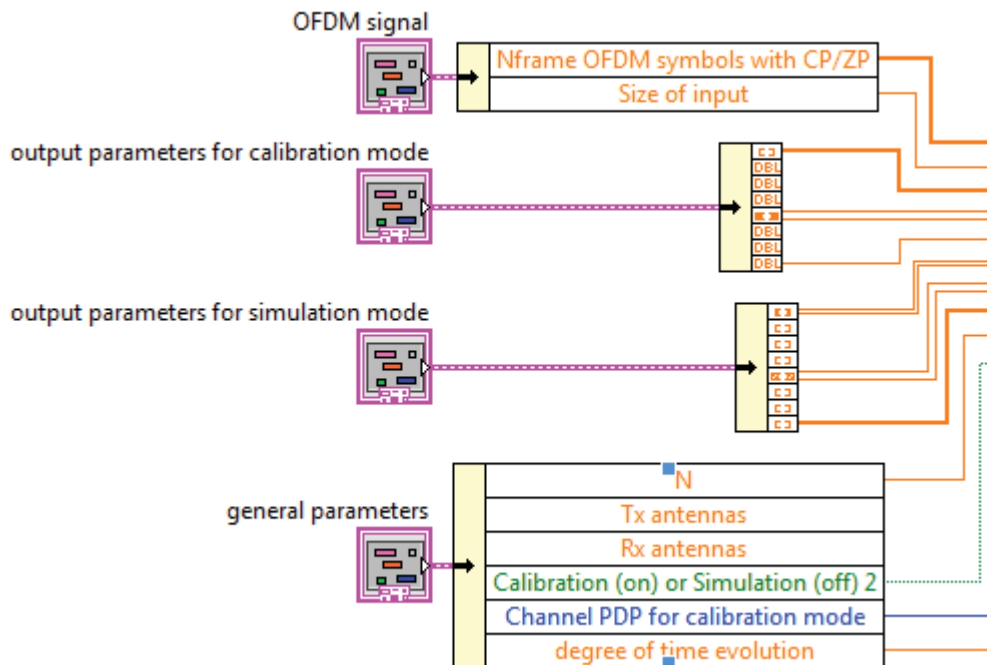
APPENDIX C



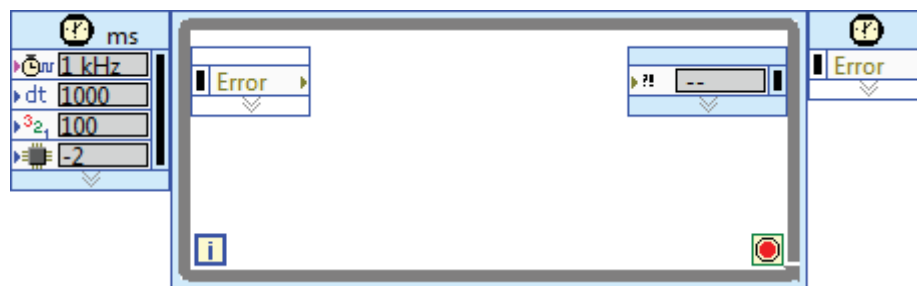
The above illustration shows the loop that generates N_{frame} number of OFDM symbols with a cyclic prefix equal to one-fourth of the FFT size. The IFFT VI can be found in the middle of the loop. The input symbol stream consists of 4-QAM symbols which are grouped 96 at a time, FFT-shifted, appended with 16 zeros on either side to form a 128 length vector, and then passed to the IFFT VI. Then, the cyclic prefix is attached following which it is 'stored' at the loop boundary (a process referred to as loop indexing) until all ' N_{frame} ' symbols have been generated. The output of the loop is a vector of length = $N_{frame} * (\text{IFFT size} + \text{cyclic prefix length}) = N_{frame} * 160$.

APPENDIX D

Input clusters to the emulator VIs:

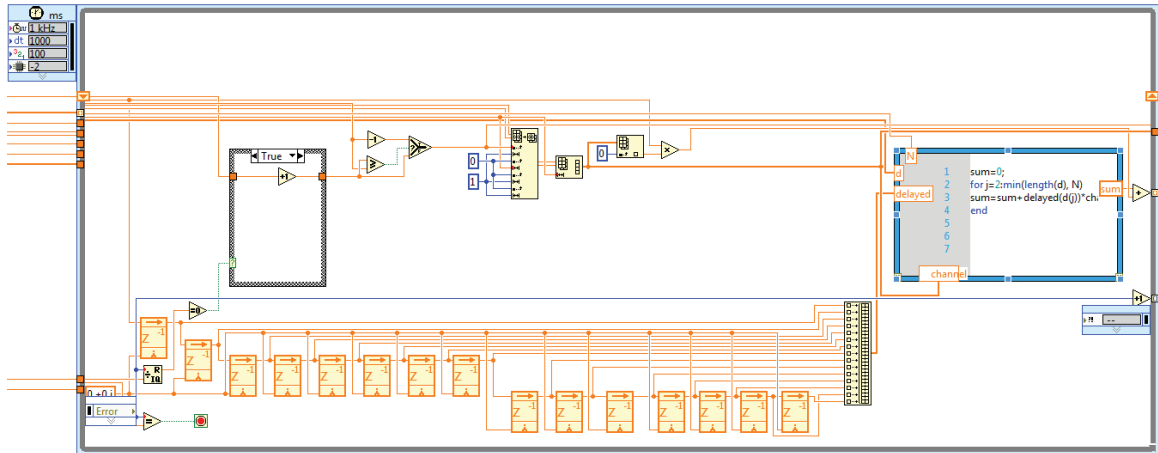


A timed loop:



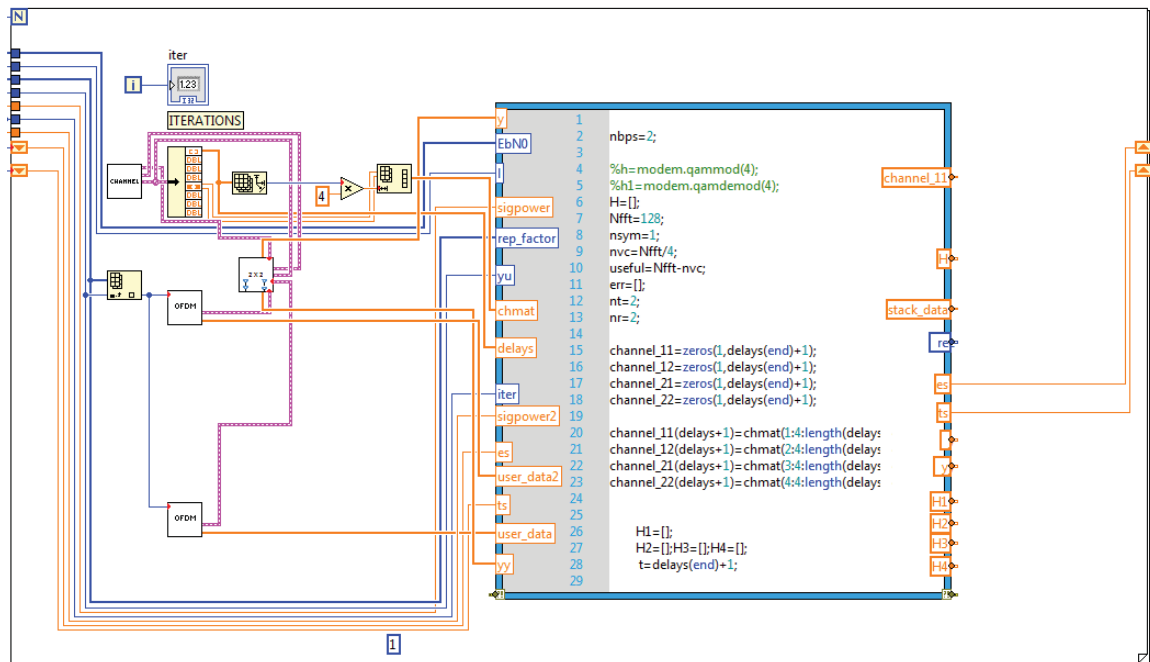
The box on the left side of the loop controls the input options to the timed loop. The important ones here are the clock rate, the time-step of the loop, denoted by 'dt', and the virtual priority number of this timed loop with respect to all other timed loops in the VI. -2 refers to the processor number in use.

Illustration of a single sub-channel in an emulator:



The above illustration shows data wires from the input clusters entering the timed loop of a single sub-channel in an emulator. The timed loop has a red 'stop' button that is conditionally activated. There are 15 delay elements. Each delay element delays the input sample by the specified 'dt' in the input-options box on the left. The code in the MathScript window performs the multiplication and accumulation operation. Here, since the delays are user-supplied and varying randomly (but within 15 sample instants) at the start of each execution, all the delayed samples are first grouped together and then the appropriate input sample and channel coefficient pairs are multiplied and added.

APPENDIX E



The above illustration shows the loop that runs over the number of iterations for the system-measurements VI for a MIMO emulator. Two OFDM sources generate test signals for each of the 2 antennas and these are passed as input to the '2 x 2' VI in the left-center of the figure. This is the MIMO emulator which also accepts an input from the channel VI. The output from the 2 x 2 VI is passed to the MathScript node which implements the receiver and calculates the average BER.

Every time the system-emulator VI is run, the above sub-VIs are executed for each iteration for every average BER value. The receiver runs and the number of errored bits are accumulated over the iterations using shift registers (the yellow arrows on the left and the right borders of the loop). The average error rate is in turn stored for every BER value and returned at the end of the VI execution. This is manually exported to MATLAB for plotting.

REFERENCES

- [1] To-Ping Wang, Chun-Hao Liao and Tzi-Dar Chiueh, "A Real-Time Digital Baseband MIMO Channel Emulation System."
- [2] Hamid Eslami and Ahmed M. Eltawil, "A Real-Time Wireless Channel Emulator For MIMO Systems."
- [3] Hamid Eslami, Sang V. Tran and Ahmed M. Eltawil, "Design and Implementation of a Scalable Channel Emulator for Wideband MIMO Systems", *IEEE Transactions on Vehicular Technology*, Vol.58, No. 9, November 2009.
- [4] Chih-Cheng Fu, To-Ping Wang, Kang-Chuan Chang, Chung-Hao Liao and Tzi-Dar Chiueh, "A Real-Time Digital Baseband Channel Emulation System for OFDM Communications."
- [5] Hao Xu , Dmitry Chizhik, Howard Huang and Reinaldo Valenzuela, "A Generalized Space–Time Multiple-Input Multiple-Output (MIMO) Channel Model", *IEEE Transactions on Wireless Communications*, Vol. 3, No. 3, May 2004.
- [6] Laurent Schumacher , Klaus I. Pedersen and Preben E. Mogensen, "From Antenna Spacings to Theoretical Capacities - Guidelines for simulating MIMO systems", *IEEE PIMRC 2002*.
- [7] 3rd Generation Partnership Project; Technical Specification Group Radio Access Network; Spatial channel model for Multiple Input Multiple Output (MIMO) simulations (Release 10) 3GPP TR 25.996 V10.0.0(2011-03).
- [8] Yong Soo Cho, Jaekwon Kim, Won Young Yang and Chung G. Kang, *MIMO-OFDM WIRELESS COMMUNICATIONS WITH MATLAB* , IEEE Press, 2010.
- [9] W. Lee, "Effects on Correlation Between Two Mobile Radio Base-Station Antennas," *IEEE Transactions on Communications*, vol. 21, pp. 1214-1224, Nov. 1973.
- [10] J.Fuhl, A.F. Molisch and E.Bonek, " Unified Channel Model for Mobile Radio Systems with Smart Antennas", *IEEE Proceedings - Radar, Sonar Navigation*, Vol. 145, pp. 33-41, Feb. 1998.
- [11] Daniel S. Baum, Jan Hansen, Giovanni Del Galdo, Marko Milojevic, Jari Salo and Pekka Kyösti, "An Interim Channel Model for Beyond-3G Systems Extending the 3GPP Spatial Channel Model (SCM)", *VTC 2005-Spring*.

[12] Ivan Cibrario Bertolotti, "Real-Time Operating Systems Tutorial", ISIE 2010.

[13] LabVIEW Real-Time Application Development Course Manual, National Instruments Corporation 2009.